Periodic envelopes of waves over non-uniform depth

Girish K. Rajan,[1] Saziye Bayram,[2] and Diane M. Henderson[1]

[1)] *W. G. Pritchard Fluid Mechanics Laboratory, Department of Mathematics, Penn State University, PA 16802, USA*

[2)] *Mathematics Department, State University of New York Buffalo, NY 14222, USA*

(Dated: 8 February 2016)

The envelope of narrow-banded, periodic, surface-gravity waves propagating in one dimension over water of finite, non-uniform depth may be modeled by the Djordjević and Redekopp[1] equation (DRE). Here we find five approximate solutions of the DRE that are in the form of Jacobi elliptic functions and discuss them within the framework of ocean swell. We find that in all cases, the maximum envelope-amplitude decreases/increases when the wave group propagates on water of decreasing/increasing depth. In the limit of the elliptic modulus approaching one, three of the solutions reduce to the envelope soliton solution. In the limit of the elliptic modulus approaching zero, two of the solutions reduce to an envelope-amplitude that is uniform in an appropriate reference frame.

PACS numbers: Valid PACS appear here
Keywords: Suggested keywords

I. INTRODUCTION

Here, we investigate the envelopes of narrow-banded, periodic, surface-gravity (carrier) waves propagating in one horizontal dimension on water of variable depth. We consider carrier waves for which the local wavenumber, k, and local depth, h, are such that kh is small enough for the carrier waves to be in finite depth, but $kh > 1.363$ over the entire interval of propagation. Such wave groups result, for example, from ocean swell propagating from deep water onto the continental shelf, as discussed in §IV. Djordjević and Redekopp[1] considered carrier waves in this regime propagating over a slowly-varying bathymetry and derived an evolution equation for their complex wave envelope, $A(x,\tau)$,

$$\mathrm{i}\left[\frac{\partial A}{\partial x} + \hat{\mu}(x)A\right] + \alpha(x)\frac{\partial^2 A}{\partial \tau^2} + \beta(x)|A|^2 A = 0, \tag{1}$$

where

$$x = \hat{\epsilon}^2 X, \tag{2a}$$

$$\tau = \hat{\epsilon}\left[\int^X \frac{\mathrm{d}X}{c_g(x)} \; - \; T\right], \tag{2b}$$

represent slow space and time scales, $\hat{\epsilon} \ll 1$ indicates weak nonlinearity, $c_g(x)$ is the group velocity, defined in (4); the coefficients $\hat{\mu}(x)$, $\alpha(x)$, and $\beta(x)$ are slowly-varying functions defined in (5), (6), and (7); and $\{X,T\}$ represent the physical space and time. The Djordjević and Redekopp equation (DRE), (1), is written such that the evolution is in space rather than time, corresponding to waves measured at fixed locations as they travel across the ocean or down a wave tank in the laboratory. The dispersion relation for these gravity waves is

$$\omega^2 = g\; k(x) \tanh\big[k(x)h(x)\big], \tag{3}$$

where g is the acceleration due to gravity, $h(x)$ is the depth, ω is the frequency of the wave, and $k(x)$ is its wavenumber. Since there is no temporal variation in the bathymetry, the carrier-wave frequency, ω, is fixed, and its wavenumber, $k(x)$, may be determined implicitly from (3), for any given depth profile, $h(x)$. The group velocity, c_g, is also obtained from (3) to be

$$c_g(x) = \frac{\mathrm{d}\omega}{\mathrm{d}k} = \frac{g}{2\omega}\Big[\tanh(kh) + kh\;\mathrm{sech}^2(kh)\Big]. \tag{4}$$

The real-valued, slowly-varying coefficients (see Djordjević and Redekopp[1]) in (1) are

$$\hat{\mu}(x) = \left[\frac{(1-\sigma^2)\,(1-kh\sigma)}{\sigma + kh\,(1-\sigma^2)}\right]\left[\frac{\mathrm{d}\,(kh)}{\mathrm{d}x}\right] \equiv \frac{1}{2c_g}\left(\frac{\mathrm{d}c_g}{\mathrm{d}x}\right), \tag{5}$$

$$\alpha(x) = \frac{-1}{2\omega c_g}\left[1 - \frac{gh}{{c_g}^2}\left(1-\sigma^2\right)(1-kh\sigma)\right], \tag{6}$$

$$\beta(x) = \frac{-g^2k^4}{4\omega^3\sigma^2 c_g}\left\{9 - 10\sigma^2 + 9\sigma^4 - \frac{2\sigma^2}{gh - {c_g}^2}\left[4{c_p}^2 + 4c_pc_g\left(1-\sigma^2\right) + gh\big(1-\sigma^2\big)^2\right]\right\}, \tag{7}$$

where

$$c_p(x) = \frac{\omega}{k(x)} \tag{8}$$

is the phase velocity and

$$\sigma(x) = \tanh(kh). \tag{9}$$

The expression, (7), for the coefficient β agrees with (2.17) of Djordjević and Redekopp[1], except for a typo in the last term, which is corrected here (private communication with Redekopp (2011)). For more details on obtaining (7), see §1.4 of Rajan[2] (pp 5-9).

For the case of $kh < 1.363$, Grimshaw[3,4] analyzed the deformation of a solitary wave due to slow variation of the bathymetry. He predicted that solitary wave amplitudes vary inversely with depth. In contrast, for the case of $kh > 1.363$, Benilov, Flanagan, and Howlin[5] used the DRE and found that both the envelope-amplitude and envelope-width of the wave group decreased with decreasing depth. At $kh \approx 1.363$, the coefficient of the nonlinear term in the governing equation (1) vanishes (as shown in Fig. 1). See Grimshaw and Annenkov[6] for equations that are valid for $kh \approx 1.363$, which corresponds to the boundary of the Benjamin-Feir[7] instability.

One reason that understanding the evolution of waves propagating on variable bathymetry has grown in interest in recent years is because of results that have shown that the variable bathymetry can influence the formation of freak waves. In particular, Janssen and Onorato[8] pointed out that the Draupner freak wave (the first freak wave for which there is a measured time series of surface displacements) probably occurred in a dimensionless depth of kh between 1.2 and 4. Zeng and Trulsen[9] used a modified DRE-type equation (see Zeng and Trulsen[9] for a review of enhancements to the DRE equations) to find that the bathymetry can cause a spatially non-uniform distribution of freak waves, unlike the uniform distribution that is expected to occur on uniform depth. Experiments with irregular,

long-crested waves by Trulsen, Zeng, and Gramstad[10] showed the effects of a sloping bottom (and weak nonlinearity) on spectral statistics and found there can be a maximum probability of a large wave envelope on the shallower side of the slope. A numerical investigation by Gramstad *et al.*[11] using a Boussinesq-type model gave results in agreement with these experiments.

Here we consider the periodic case for $kh > 1.363$. We identify five exact, periodic Jacobi elliptic functions (see Appendix A) that satisfy the uniform-depth version of the DRE. In §III we consider one of these envelope solutions, the Jacobi-cn function, and use asymptotics to determine how its maximum amplitude varies due to a slowly-varying depth profile. We present similar results for the other elliptic function solutions. In the limit of the elliptic modulus approaching one, three of these five functions reduce to the soliton solution found by Benilov, Flanagan, and Howlin[5]. In the limit of the elliptic modulus approaching zero, two of these functions reduce to a solution whose amplitude is uniform in an appropriate reference frame, discussed in Rajan[2] (see Chapter 2, pp 15-32).

II. EVOLUTION EQUATIONS

Motivated by Benilov, Flanagan, and Howlin[5], we consider carrier waves whose envelope-amplitudes vary on a spatial scale,

$$\xi = \epsilon\, x, \tag{10}$$

which is slow compared to the slow scale x (see (2a)). This scale accounts for changes in bathymetry that are slow compared to the spatial scale of the envelope. So here, changes in bathymetry are slow compared to the envelope as well as the carrier wave. Using (10) in (1) results in

$$\mathrm{i}\left[\epsilon\frac{\partial A}{\partial \xi} + \epsilon\mu(\xi)A\right] + \alpha(\xi)\left(\frac{\partial^2 A}{\partial \tau^2}\right) + \beta(\xi)|A|^2 A = 0, \tag{11}$$

where one may apply (5) and (10) to see that

$$\mu(\xi) := \frac{\hat{\mu}(x)}{\epsilon} = \left[\frac{(1-\sigma^2)\,(1-kh\sigma)}{\sigma + kh\,(1-\sigma^2)}\right]\left[\frac{\mathrm{d}\,(kh)}{\mathrm{d}\xi}\right] \equiv \frac{1}{2c_g}\left(\frac{\mathrm{d}c_g}{\mathrm{d}\xi}\right). \tag{12}$$

FIG. 1. The coefficients (a) α and (b) β, nondimensionalized, as functions of kh. The vertical dashed lines are $kh = 1.363$.

We note that (11) admits two conserved quantities,

$$M_A = \int_D c_g(\xi)|A|^2 \mathrm{d}\tau, \tag{13a}$$

$$P_A = \int_D c_g(\xi)\big[AA^*{}_\tau - A_\tau A^*\big]\mathrm{d}\tau, \tag{13b}$$

for which $\mathrm{d}M_A/\mathrm{d}\xi = 0$, $\mathrm{d}P_A/\mathrm{d}\xi = 0$, the $*$ indicates complex conjugate, and D is one (time) period of the wave envelope. The period, D, remains constant during wave evolution, due to the absence of a temporal variation in the bathymetry. For the propagation of surface gravity carrier waves at a fixed frequency, ω, using (3), (4), (8), (9), and (10), the coefficients α and β in (6) and (7) may be written as functions of kh such that

$$\alpha\Big(k(\xi)h(\xi)\Big) = \left(\frac{-1}{g}\right)\left(\frac{1}{\chi}\right)\left\{1 - \left[\frac{4kh\sigma\big(1-\sigma^2\big)\big(1-kh\sigma\big)}{\chi^2}\right]\right\}, \tag{14}$$

$$\beta\Big(k(\xi)h(\xi)\Big) = \frac{-\omega^6}{2g^3\sigma^6\chi}\left\{9-10\sigma^2+9\sigma^4-8\sigma^2\left[\frac{4\sigma^2+2\sigma\big(1-\sigma^2\big)\chi+kh\sigma\big(1-\sigma^2\big)^2}{4kh\sigma-\chi^2}\right]\right\}, \tag{15}$$

where

$$\chi\Big(k(\xi)h(\xi)\Big) = \sigma + kh\big(1-\sigma^2\big). \tag{16}$$

The coefficients α and β defined in (14) and (15) are shown as dimensionless functions of kh in Fig. 1. Figure 1(a) shows that $\alpha < 0$ for all values of kh, and reaches a limiting value of $\alpha = -1/g$ for $kh \to \infty$. From (14) and (16), one can also see that $\alpha \to 0$ when $kh \to 0$. Figure 1(b) shows that the coefficient β changes sign at $kh \approx 1.363$, with $\beta > 0$ for $kh < 1.363$ and $\beta < 0$ for $kh > 1.363$. In this work, since we focus on $kh > 1.363$, the coefficients α and β are both negative so that the ratio $\beta/\alpha > 0$. The coefficient μ, defined in (12), leads to growth (if $\mu < 0$) or decay (if $\mu > 0$), and is zero if the bathymetry is uniform. To see the growth or decay, consider (13a). Since $\mathrm{d}M_A/\mathrm{d}\xi = 0$, it follows that

$$\frac{\mathrm{d}E}{\mathrm{d}\xi} = -\frac{E}{c_g}\left(\frac{\mathrm{d}c_g}{\mathrm{d}\xi}\right), \tag{17}$$

where

$$E(\xi) = \int_D \left|A(\xi,\tau)\right|^2 \mathrm{d}\tau, \tag{18}$$

represents the energy in one period, D, of the wave envelope. The group velocity, $c_g > 0$, so that the growth/decay of E depends on $\mathrm{sgn}(\mathrm{d}c_g/\mathrm{d}\xi)$, which is related to $\mathrm{sgn}(\mathrm{d}h/\mathrm{d}\xi)$ as discussed below. Using (10) and the dispersion relation, (3), we obtain

$$\frac{\mathrm{d}k}{\mathrm{d}\xi} = \frac{-gk^2\left(1-\sigma^2\right)}{2\omega c_g}\left(\frac{\mathrm{d}h}{\mathrm{d}\xi}\right), \tag{19}$$

for carrier waves of fixed frequency, ω. Similarly, using (10), (3), (4), and (12), the group velocity may be related to the slope of the bathymetry by

$$2\mu c_g = \frac{\mathrm{d}c_g}{\mathrm{d}\xi} = \frac{\left(1-\sigma^2\right)\left(1-kh\sigma\right)}{\sigma + kh\left(1-\sigma^2\right)}\left(\frac{gk\sigma}{\omega}\right)\frac{\mathrm{d}h}{\mathrm{d}\xi}. \tag{20}$$

The term $(1-kh\sigma)$ changes sign at $kh \approx 1.2$. Therefore, (20) implies that

$$\frac{\mathrm{d}c_g}{\mathrm{d}\xi} \sim +\frac{\mathrm{d}h}{\mathrm{d}\xi} \quad \text{if} \quad kh \lesssim 1.2, \tag{21a}$$

$$\frac{\mathrm{d}c_g}{\mathrm{d}\xi} \sim -\frac{\mathrm{d}h}{\mathrm{d}\xi} \quad \text{if} \quad kh \gtrsim 1.2. \tag{21b}$$

Since $kh > 1.363$ in this analysis, we use (21b), along with (17), (19), (20), to obtain two cases for carrier waves of fixed frequency, ω:

$$\frac{\mathrm{d}h}{\mathrm{d}\xi} < 0 \quad \Rightarrow \quad \frac{\mathrm{d}k}{\mathrm{d}\xi} > 0 \ \text{ and } \ \mu \sim \frac{\mathrm{d}c_g}{\mathrm{d}\xi} > 0 \quad \Rightarrow \quad \frac{\mathrm{d}E}{\mathrm{d}\xi} < 0, \tag{22a}$$

$$\frac{\mathrm{d}h}{\mathrm{d}\xi} > 0 \quad \Rightarrow \quad \frac{\mathrm{d}k}{\mathrm{d}\xi} < 0 \ \text{ and } \ \mu \sim \frac{\mathrm{d}c_g}{\mathrm{d}\xi} < 0 \quad \Rightarrow \quad \frac{\mathrm{d}E}{\mathrm{d}\xi} > 0. \tag{22b}$$

Therefore, (22a) shows that wave groups traveling on water of decreasing depth have envelopes of decreasing energy, and (22b) shows that wave groups traveling on water of increasing depth have envelopes of increasing energy. Benilov, Flanagan, and Howlin[5] observed this general result in a numerical simulation using an envelope soliton for initial data. Relations (22) provide an explanation for their numerical result. Rajan[2] (Chapter 2, pp 15-32) discuss the effect of the sign of the coefficient μ on the stability of a uniform-amplitude wavetrain propagating on water of variable depth.

For a uniform bathymetry, we note that the coefficients α, β, ν are constants, and $\mu \equiv 0$. The uniform-depth version, (A1), of the DRE, (1), is given in appendix A. There, we also identify five exact, periodic solutions of (A1). The solutions are in the form of Jacobi-elliptic functions, and are listed in Table IV. We use these solutions as a starting point in §III.

III. ASYMPTOTIC ANALYSIS

In this section, we obtain expressions for the evolution of the envelope-width and the envelope-amplitude of a wave group, following the procedure outlined in Benilov, Flanagan, and Howlin[5]. The goal is to determine how the maximum envelope-amplitude and the envelope-width change with changing depth.

A. Approximate envelope solutions

Equation (A10) is a general form of five exact solutions for $A(\xi,\tau)$ that satisfy the uniform-depth version, (A1), of the DRE. We account for a slowly-varying bathymetry by allowing the complex envelope, $A(\xi,\tau)$, to vary slowly so that

$$A(\xi,\tau) = B(\xi,\tau)\ \exp\left\{ \mathrm{i}\int^{\xi} c_2(s)\mathrm{d}s \right\}, \tag{23}$$

where c_2 is defined in Table IV. Here, we present the asymptotic analysis for one of the five cases, the Jacobi-cn solution (case #1 of Table IV), for which

$$c_2(s) = \frac{1}{\epsilon}\left\{ \left[2m^2(s)-1\right]\ \alpha(s)\ \lambda^2(s) \right\}, \tag{24}$$

where $m(\xi)$ is the elliptic modulus (see p.9 of Byrd and Friedman[12]) and $\lambda(\xi)$ is the frequency of the envelope. Then, we will generalize the results of the asymptotic analysis to the other cases listed in Table IV.

For case #1 of Table IV, substituting (24) in (23), we obtain

$$A(\xi,\tau) = B(\xi,\tau)\ \exp\left\{ \frac{\mathrm{i}}{\epsilon}\int^{\xi} \Big(2m^2-1\Big)\alpha\lambda^2\mathrm{d}s \right\}, \tag{25}$$

where the parameters α, λ, and m are functions of ξ as a result of the varying depth. Substituting (25) in (11), we obtain

$$-\alpha\lambda^2(2m^2-1)B + \alpha B_{\tau\tau} + \beta|B|^2B = \epsilon\left[-\mathrm{i}B_{\xi} - \mathrm{i}\mu B \right]. \tag{26}$$

Letting $m \to 1$, we obtain the equation corresponding to the soliton solution,

$$-\alpha\lambda^2 B + \alpha B_{\tau\tau} + \beta|B|^2B = \epsilon\left[-\mathrm{i}B_{\xi} - \mathrm{i}\mu B \right], \tag{27}$$

which is equation (3.8) of Benilov, Flanagan, and Howlin[5] with their $\nu = 0$, and with the first term corrected here. We expand B in an asymptotic series in ϵ such that

$$B(\xi,\tau) = B_0(\xi,\tau) + \epsilon B_1(\xi,\tau) + \mathcal{O}\left(\epsilon^2\right). \tag{28}$$

Substituting (28) in (26), we obtain

$$\begin{aligned} -\alpha\lambda^2(2m^2-1)B_0 - \epsilon\alpha\lambda^2(2m^2-1)B_1 + \alpha\left(B_0\right)_{\tau\tau} + \epsilon\alpha\left(B_1\right)_{\tau\tau} + \beta|B_0|^2B_0 \\ +\epsilon\beta\Big[2B_1|B_0|^2 + {B_1}^*{B_0}^2\Big] = \epsilon\Bigg[-\mathrm{i}\left(B_0\right)_\xi - \mathrm{i}\mu B_0\Bigg] + \mathcal{O}\left(\epsilon^2\right). \end{aligned} \tag{29}$$

Grouping together terms at $\mathcal{O}(\epsilon^0)$ and at $\mathcal{O}(\epsilon^1)$ in (29), we obtain

$$-\alpha\lambda^2(2m^2-1)B_0 + \alpha\left(B_0\right)_{\tau\tau} + \beta|B_0|^2B_0 = 0, \tag{30}$$

and

$$-\alpha\lambda^2(2m^2-1)B_1 + \alpha\left(B_1\right)_{\tau\tau} + \beta\Big[2B_1|B_0|^2 + {B_1}^*{B_0}^2\Big] = \Bigg[-\mathrm{i}\left(B_0\right)_\xi - \mathrm{i}\mu B_0\Bigg]. \tag{31}$$

The five Jacobi-elliptic function solutions of (30), and their limiting cases are listed in Table I. Here, we show the details for the Jacobi-cn function (see #1 of Table I),

$$B_0(\xi,\tau) = m\ \lambda\ \sqrt{\frac{2\alpha}{\beta}}\ \ \mathrm{cn}\left(\lambda\tau; m\right)\ \ \in\ \mathbb{R}, \tag{32}$$

where the period of the envelope is

$$D = \frac{4K(m)}{\lambda} = \text{constant} \in \mathbb{R}, \tag{33}$$

and $K(m)$ is the complete elliptic integral of the first kind. The period D is a constant because there is no temporal variation in the bathymetry. The goal is to determine how $m(\xi)$ and $\lambda(\xi)$ (and consequently the maximum envelope-amplitude) vary as a result of slowly-varying bathymetry.

Substituting

$$B_1(\xi,\tau) = B_{1r}(\xi,\tau) + \mathrm{i}B_{1i}(\xi,\tau) \tag{34}$$

in (31) and separating the real and imaginary parts, we obtain

$$-\alpha\lambda^2(2m^2-1)B_{1r} + \alpha\left(B_{1r}\right)_{\tau\tau} + 3\beta|B_0|^2B_{1r} = 0, \tag{35}$$

and

$$-\alpha\lambda^2(2m^2-1)B_{1i} + \alpha\left(B_{1i}\right)_{\tau\tau} + \beta|B_0|^2B_{1i} = -\Big[\left(B_0\right)_\xi + \mu B_0\Big]. \tag{36}$$

Consider the homogeneous version of (36),

$$-\alpha\lambda^2(2m^2-1)B_{1i}+\alpha\left(B_{1i}\right)_{\tau\tau}+\beta|B_0|^2B_{1i}=0. \tag{37}$$

Differentiating (30) with respect to τ, and using $|B_0|^2=(B_0)^2$ (see (32)), we obtain

$$-\alpha\lambda^2(2m^2-1)\left(B_0\right)_\tau+\alpha\left(B_0\right)_{\tau\tau\tau}+3\beta\left(B_0\right)^2\left(B_0\right)_\tau=0. \tag{38}$$

Comparing (35) with (38) and (30) with (37), we obtain

$$B_{1r}=\left(B_0\right)_\tau \qquad \text{and} \qquad B_{1i}=B_0. \tag{39}$$

The operator in the linear, non-homogeneous, ordinary differential equation (36) is self-adjoint. The Fredholm Alternative theorem dictates that (36) has a bounded solution if and only if its right-hand side is orthogonal to the solution of its homogeneous version, (37). It follows that

$$\int_{-D/2}^{D/2}\Big[\left(B_0\right)_\xi+\mu B_0\Big]B_0\mathrm{d}\tau=0. \tag{40}$$

Rewriting (40) as

$$\frac{\mathrm{d}}{\mathrm{d}\xi}\left[\int_{-D/2}^{D/2}\left(B_0\right)^2\mathrm{d}\tau\right]+2\mu(\xi)\int_{-D/2}^{D/2}\left(B_0\right)^2\mathrm{d}\tau=0, \tag{41}$$

and integrating, we obtain

$$\left\{\exp\Big[\int 2\mu(\xi)\mathrm{d}\xi\Big]\right\}\int_{-D/2}^{D/2}\left(B_0\right)^2\mathrm{d}\tau=\text{constant}. \tag{42}$$

Substituting (12) for $\mu(\xi)$ and (32) for B_0 in (42), and simplifying, we obtain

$$\frac{m\lambda\alpha}{\beta}\Big[E(m)+(m-1)K(m)\Big]\Big[\tanh(kh)+kh\ \mathrm{sech}^2(kh)\Big]=C_2, \tag{43}$$

where the parameters $\alpha,\ \beta,\ \lambda,\ h,\ k,$ and m are real-valued functions of ξ, $C_2\in\mathbb{R}$ is a constant, and $E(m)$ is the complete elliptic integral of the second kind. In summary, one approximate solution to the DRE, (1), is

$$A(\xi,\tau)\approx\Big[B_0(\xi,\tau)+\epsilon B_1(\xi,\tau)\Big]\ \exp\left\{\mathrm{i}\int^\xi c_2(s)\mathrm{d}s\right\}, \tag{44}$$

where c_2 is defined in (24), and B_0, B_1 are given in (32), (34), and (39). In §III B, we show how to use (33) and (43) to determine the variation of the (approximate) maximum of the envelope-amplitude, $A(\xi,\tau)$, as the depth changes with the distance of propagation.

Corresponding results for the other four Jacobi-elliptic function solutions (see Table I) can be obtained in a similar manner. Analogous results for (32), (43), and (33) are as follows.

- (a) For the Jacobi-dn function (#2 of Table I),

$$B_0(\xi,\tau) = \lambda\sqrt{2\alpha/\beta}\,\mathrm{dn}\,(\lambda\tau;m)\,, \tag{45}$$

$$\frac{\lambda\alpha}{\beta}E(m)\Big[\tanh(kh)+kh\,\mathrm{sech}^2(kh)\Big] = C_3 \;\;;\;\; D=\frac{2K(m)}{\lambda}. \tag{46}$$

- (b) For the Jacobi-nd function (#3 of Table I),

$$B_0(\xi,\tau) = \lambda\sqrt{2\alpha\,(1-m^2)/\beta}\,\mathrm{nd}\,(\lambda\tau;m)\,, \tag{47}$$

$$\frac{\lambda\alpha}{\beta}(1+m)E(m)\Big[\tanh(kh)+kh\,\mathrm{sech}^2(kh)\Big] = C_4 \;\;;\;\; D=\frac{2K(m)}{\lambda}. \tag{48}$$

- (c) For the Jacobi-sd function (#4 of Table I),

$$B_0(\xi,\tau) = m\lambda\sqrt{2\alpha\,(1-m^2)/\beta}\,\mathrm{sd}\,(\lambda\tau;m)\,, \tag{49}$$

$$\frac{m(1+m)\lambda\alpha}{\beta}\Big[(1-m)K(m)-E(m)\Big]\Big[\tanh(kh)+kh\,\mathrm{sech}^2(kh)\Big] = C_5 \;\;;\;\; D=\frac{4K(m)}{\lambda}. \tag{50}$$

- (d) For the combined Jacobi-nd and Jacobi-dn functions (#5 of Table I),

$$B_0(\xi,\tau) = \lambda\sqrt{2\alpha/\beta}\Big[\sqrt{1-m^2}\,\mathrm{nd}(\lambda\tau;m)+\mathrm{dn}(\lambda\tau;m)\Big]. \tag{51}$$

$$\frac{\lambda\alpha}{\beta}\Big[(m+2)E(m)+2\sqrt{1-m^2}\,K(m)\Big]\Big[\tanh(kh)+kh\,\mathrm{sech}^2(kh)\Big] = C_6 \;\;;\;\; D=\frac{2K(m)}{\lambda}. \tag{52}$$

Here, $\{C_3, C_4, C_5, C_6\}$ and D are real-valued constants. These results may also be obtained from the conserved quantities, (13). (See Benilov, Flanagan, and Howlin[5] who showed this for the soliton solution.)

B. Procedure to compute the maximum envelope-amplitude and envelope-width

Here, we describe the steps to compute the maximum envelope-amplitude, $B_{\max}(\xi)$, and envelope-width, $w(\xi)$, recognizing that (44) implies

$$\max\{A(\xi,\tau)\} \approx \max\{B_0(\xi,\tau)\} =: B_{\max}(\xi). \tag{53}$$

For each of the five envelope solutions, the steps are as follows.

(i) Choose a frequency, ω, of the carrier wave.

(ii) Choose a depth profile, $h(\xi)$.

(iii) Based on the choices in (i) and (ii), compute the wavenumber, $k(\xi)$, using (3).

(iv) Compute the coefficients, $\alpha(\xi)$ and $\beta(\xi)$ from (14) and (15), and the group velocity, $c_g(\xi)$ from (4).

(v) Choose an $m_0 := m(\xi = 0)$ and a $\lambda_0 := \lambda(\xi = 0)$.

(vi) For each of the five solutions, determine the fixed period D using m_0, λ_0, and one of (33), (46), (48), (50), or (52).

(vii) Compute $h_0 := h(\xi = 0)$ from (ii), $k_0 := k(\xi = 0)$ from (iii), and $\alpha_0 := \alpha(\xi = 0)$, $\beta_0 := \beta(\xi = 0)$ from (iv).

(viii) For each of the five solutions, determine the corresponding constant C_n ($n = 2, 3, 4, 5, 6$) using (v), (vii) and one of (43), (46), (48), (50), or (52).

(ix) For each of the five solutions, compute $m(\xi)$ and $\lambda(\xi)$ using one of (43), (46), (48), (50), or (52).

(x) Using $m(\xi)$ and $\lambda(\xi)$ computed in (ix) and $c_g(\xi)$ computed in (iv), determine the maximum envelope-amplitude, $B_{\max}(\xi)$ (see 53 and Table I), and the envelope-width, $w(\xi)$, defined as

$$w(\xi) = \frac{c_g(\xi)}{\lambda(\xi)}. \tag{54}$$

In §IV, we consider carrier waves of a specified fixed frequency, ω, propagating on water of a specified depth variation, $h(\xi)$. Then, following the steps described in (iii) - (x) above, we compute $m(\xi)$ and $\lambda(\xi)$, and show how the maximum envelope-amplitude and the envelope-width of the wave group vary with the distance measured along the direction of wave propagation for each of the five cases discussed above and listed in Table I.

C. Limiting cases

Here we consider two limiting cases. The first limiting case is for $m \to 1$. In this limit, the cn-solution, (32), the dn-solution, (45), and combined-nd/dn solution, (51), reduce to

TABLE I. A list of five Jacobi-elliptic functions, $B_0(\xi,\tau)$, that satisfy (30).

#	$J(\xi,\tau)$	$B_{\rm m}(\xi)$	$B_0(\xi,\tau)$	$\max(J)$	$B_{\max}(\xi) = B_{\rm m}\max(J)$	$\lim_{m\to 1} B_0(\xi,\tau)$	$\lim_{m\to 0} B_0(\xi,\tau)$
1	$\mathrm{cn}(\lambda\tau;m)$	$m\lambda\sqrt{\frac{2\alpha}{\beta}}$	$B_{\rm m}(\xi)J(\xi,\tau)$	1	$B_{\rm m}(\xi)$	$\lambda\sqrt{\frac{2\alpha}{\beta}}\ \mathrm{sech}(\lambda\tau)$	0
2	$\mathrm{dn}(\lambda\tau;m)$	$\lambda\sqrt{\frac{2\alpha}{\beta}}$	$B_{\rm m}(\xi)J(\xi,\tau)$	1	$B_{\rm m}(\xi)$	$\lambda\sqrt{\frac{2\alpha}{\beta}}\ \mathrm{sech}(\lambda\tau)$	$\lambda\sqrt{\frac{2\alpha}{\beta}}$
3	$\mathrm{nd}(\lambda\tau;m)$	$\lambda\sqrt{\frac{2\alpha(1-m^2)}{\beta}}$	$B_{\rm m}(\xi)J(\xi,\tau)$	$\frac{1}{\sqrt{1-m^2}}$	$\frac{B_{\rm m}(\xi)}{\sqrt{1-m^2}}$	0	$\lambda\sqrt{\frac{2\alpha}{\beta}}$
4	$\mathrm{sd}(\lambda\tau;m)$	$m\lambda\sqrt{\frac{2\alpha(1-m^2)}{\beta}}$	$B_{\rm m}(\xi)J(\xi,\tau)$	$\frac{1}{\sqrt{1-m^2}}$	$\frac{B_{\rm m}(\xi)}{\sqrt{1-m^2}}$	0	0
5	$\mathrm{dn}(\lambda\tau;m) + \left[\sqrt{1-m^2}\times \mathrm{nd}(\lambda\tau;m)\right]$	$\lambda\sqrt{\frac{2\alpha}{\beta}}$	$B_{\rm m}(\xi)J(\xi,\tau)$	1	$B_{\rm m}(\xi)$	$\lambda\sqrt{\frac{2\alpha}{\beta}}\ \mathrm{sech}(\lambda\tau)$	$2\lambda\sqrt{\frac{2\alpha}{\beta}}$

the soliton solution,

$$B_0(\xi,\tau) = \lambda\sqrt{2\alpha/\beta}\ \mathrm{sech}\,(\lambda\tau)\,. \tag{55}$$

In this limit, all of (43), (46), and (52) reduce to

$$\frac{\lambda\alpha}{\beta}\Big[\tanh(kh) + kh\ \mathrm{sech}^2(kh)\Big] = C_7, \tag{56}$$

where $C_7 \in \mathbb{R}$ is a constant. This result agrees with equation (3.17) of Benilov, Flanagan, and Howlin[5]. So, for $m \to 1$, three of the five solutions (see Table I) reduce to the soliton solution, while the other two solutions, the nd-solution and the sd-solution reduce to zero.

The second limiting case is for $m \to 0$. In this limit, the dn-solution, (45), and the nd-solution, (47), reduce to the solution

$$B_0(\xi,\tau) = \lambda\sqrt{2\alpha/\beta}, \tag{57}$$

whose amplitude is uniform in τ. This solution was studied in Rajan[2] (see Chapter 2, pp 15-32), and is similar to the uniform amplitude solution of the deep-water nonlinear Schrödinger

equation. In this limit, both (46) and (48) reduce to

$$\frac{\lambda\alpha}{\beta}\Big[\tanh(kh)+kh\,\mathrm{sech}^2(kh)\Big]=C_8, \tag{58}$$

where $C_8\in\mathbb{R}$ is a constant. So, for for $m\to 0$, two of the five solutions (see Table I) reduce to the Stokes-like uniform (in τ) amplitude solution, while two other solutions, the cn-solution and the sd-solution, reduce to zero. Here, the combined-nd/dn solution (see #5 of Table I) reduces to a Stokes-like uniform (in τ) amplitude solution with an amplitude that is twice that obtained for the dn-solution and the nd-solution in the limit $m\to 0$.

IV. RESULTS AND DISCUSSION

To obtain the maximum envelope-amplitude and the envelope-width of the wave group as functions of the distance measured along the direction of propagation, we consider a specific depth variation,

$$h(X)=h_a\Big\{1-\Delta h\,\tanh\big[\gamma\,(X-X_c)\,\big]\Big\};\quad X_0\leqslant X\leqslant X_{\max}, \tag{59}$$

where h, h_a, X, X_0, $X_{\max}$, and X_c are in m, γ is in m^{-1}, and Δh is dimensionless. To make the depth, h, a slowly varying function corresponding to oceanic scales, we choose

$$h_a=100\text{ m},\qquad \Delta h=0.08,\qquad \text{and}\qquad \gamma=10^{-4}\text{ m}^{-1}. \tag{60}$$

These choices are consistent with values corresponding to the continental shelf. For example, see Thurman[13] who gives the variation in the distance of the shelf from the shore to be from a few tens of meters to about 1300 km, its average slope to be about 0.0019, and the average depth at which the shelf breaks to the continental slope to be about 135 m. Additionally, we choose

$$X_0=0,\qquad X_c=4\times10^4\text{ m}=40\text{ km},\qquad \text{and}\qquad X_{\max}=10\times10^4\text{ m}=100\text{ km}. \tag{61}$$

According to (59), (60), and (61), the depth of water decreases along the direction of propagation, as shown in Fig. 2(a), in which the shaded region represents the solid bottom. For a 16-second carrier-wave with a frequency of $\omega=0.39\,\mathrm{s}^{-1}$, the wavenumber shown in Fig. 2(b) is obtained implicitly from (3). Then, the depth variation corresponds to the condition $kh>1.363$ throughout the interval of propagation. Figure 2(c) shows the $kh-$variation to

be consistent with this condition. Figures 2(e) and 2(f) show that α and β are negative in this interval, also consistent with this condition. Figure 2(d) shows the variation of the group velocity, c_g. The sign of $\mathrm{d}c_g/\mathrm{d}\xi$ determines whether the energy increases/decreases spatially according to (17). Thus, Fig. 2(d) shows that the energy will decrease for all solutions during propagation into shallower water, consistent with (22a). If l represents the typical length of the carrier wave, and L is a horizontal length scale over which the water depth varies significantly (see Fig. 2), then over the interval of propagation,

$$365 < l = \frac{2\pi}{k} < 380 \text{ m} \quad \text{and} \quad L \equiv \gamma^{-1} = 10^4 \text{ m}. \tag{62}$$

Thus the carrier wave has to travel about 27 wavelengths to physically cover the distance, L, and about 270 wavelengths to cover the entire 100 km interval. We define the dimensionless parameter ϵ to be a ratio of the envelope-width to the length scale over which the water depth varies significantly, so that

$$\epsilon := \frac{w(\xi)}{L}. \tag{63}$$

From (54), $w(\xi = 0) = 943.33$ m if $\lambda_0 = 0.015$ and $w(\xi = 0) = 471.66$ m if $\lambda_0 = 0.030$. Then, using (62) and (63), we obtain $\epsilon = 0.094$ or 0.047 when $\xi = 0$. We choose $\epsilon = 0.1$ for the computations of all five solutions.

For the depth variation given in (59), Fig. 3 shows the parameters m, λ, and B_{m} (see Table I) as functions of the distance measured along the direction of propagation. The initial values, m_0 and λ_0, are listed in Table II. As shown there, $m_0 = 0.999$ for all five cases, while

FIG. 2. The slowly-varying parameters as functions of the distance along the direction of propagation. The depth of water shown in (a) varies according to (59), with the shaded region representing the solid bottom. The wave propagation is from deeper ($h = 108$ m and $kh \approx 1.8$ at $X_0 = 0$) water to shallower ($h = 92$ m and $kh \approx 1.6$ at $X_{\max} = 100$ km) water. The period of the carrier waves is 16 s, and its frequency is $\omega = 0.39$ s^{-1}.

FIG. 3. The parameters m, λ, and $B_{\rm m}$ as functions of the distance along the direction of propagation for $\omega = 0.39$ s^{-1}. Each row corresponds to one of the five Jacobi-elliptic solutions of (30). Panels (a) - (c) correspond to case #1, (d) - (f) correspond to case #2, (g) - (i) correspond to case #3, (j) - (l) correspond to case #4, and (m) - (o) correspond to case #5, as listed in Tables I and II. Note that the scales on the ordinate differ for each row.

TABLE II. Initial values, $m_0 := m(\xi = 0)$ and $\lambda_0 := \lambda(\xi = 0)$; the periods, D; and numerical values of the constants $\{C_2, C_3, C_4, C_5, C_6\}$, for each of the five Jacobi-elliptic functions, $B_0(\xi, \tau)$, that satisfy (30). The numbers are computed based on (59), (60), and (61), using the steps described in §III B.

#	$B_0(\xi,\tau)$	m_0	λ_0 $\left(\text{s}^{-1}\right)$	Period D (s)	Constant $\left(\text{m}^2\text{s}\right)$	$m(\xi)$, $\lambda(\xi)$ obtained from
1	$B_{\rm m}\ \text{cn}(\lambda\tau; m)$	0.999	0.030	$\frac{4K(m_0)}{\lambda_0} = 599.4$	$C_2 = 773.10$	(43), (33)
2	$B_{\rm m}\ \text{dn}(\lambda\tau; m)$	0.999	0.015	$\frac{2K(m_0)}{\lambda_0} = 599.4$	$C_3 = 388.68$	(46)
3	$B_{\rm m}\ \text{nd}(\lambda\tau; m)$	0.999	0.015	$\frac{2K(m_0)}{\lambda_0} = 599.4$	$C_4 = 776.97$	(48)
4	$B_{\rm m}\ \text{sd}(\lambda\tau; m)$	0.999	0.030	$\frac{4K(m_0)}{\lambda_0} = 599.4$	$C_5 = -1545.4$	(50)
5	$B_{\rm m}\Big[\text{dn}(\lambda\tau; m) + \sqrt{1-m^2}\ \text{nd}(\lambda\tau; m)\Big]$	0.999	0.015	$\frac{2K(m_0)}{\lambda_0} = 599.4$	$C_6 = 1321.3$	(52)

the value of λ_0 is chosen so that the period, D, is the same for all five solutions. Figure 3 shows that both m and λ decrease with propagation distance for all five cases. $B_{\rm m}$ decreases with propagation distance for three of the five cases, and increases with distance for the remaining two: the Jacobi-nd and Jacobi-sd solutions (cases #3 and #4 of Tables I and II). We note that the maximum envelope-amplitude, $B_{\rm max} = B_{\rm m}\ \max(J)$, so that this variation in $B_{\rm m}$ does not by itself determine the variation in $B_{\rm max}$.

Figures 4 and 5 show the variation in the maximum envelope-amplitude, $B_{\rm max}$, and the envelope-width, w, of a wave group propagating on water whose depth decreases according to (59). Figure 4 shows that the maximum envelope-amplitude decreases with decreasing depth,

FIG. 4. The relative maximum envelope-amplitude of a wave group as a function of the distance along the direction of propagation for $\omega = 0.39$ s^{-1}. Each case corresponds to one of the five Jacobi-elliptic solutions of (30), listed in Tables I and II.

while Fig. 5 shows that the envelope-width increases with decreasing depth, for all five cases. The largest reduction ($\sim 58\%$) in the maximum envelope-amplitude, and correspondingly the largest growth ($\sim 188\%$) in the envelope-width was observed for case #5, the combined dn and nd functions, whereas the smallest reduction ($\sim 17\%$) in the maximum envelope-amplitude, and correspondingly the smallest growth ($\sim 45\%$) in the envelope-width was observed for case #4, the Jacobi-sd function (see Table II). Since $E(\xi) \propto B_{\max}(\xi)$, this reduction in the maximum envelope-amplitude with decreasing depth is consistent with (22a). Figure 6 presents the initial ($X = X_0$) and final ($X = X_{\max}$) surface displacements. The maximum surface displacement at $X = X_{\max}$ is lesser than that at $X = X_0$ for all five cases. These results are consistent with the variations shown in Fig. 4, which shows the surface displacement as a function of propagation distance for one period of the envelope solutions.

FIG. 5. The relative envelope-width of a wave group as a function of the distance along the direction of propagation for $\omega = 0.39$ s^{-1}. Each case corresponds to one of the five Jacobi-elliptic solutions of (30), listed in Tables I and II.

FIG. 6. Time series of surface displacements, $\eta(X,T) \approx \mathrm{Re}\left\{\epsilon A(X,T)\exp\left[\mathrm{i}\left(\int^X k(s)\mathrm{d}s - \omega T\right)\right]\right\}$, where $A(X,T)$ is obtained from (44) using $\epsilon = \hat{\epsilon} = 0.1$. Each panel shows η (grey curve), $\pm\mathrm{Re}(\epsilon A)$ (black solid/dotted curve). Row (n) corresponds to solution $\#n$ in Table I with $n = 1, 2, 3, 4, 5$. Columns (a) and (b) correspond to $X = X_0$ and $X = X_{\max}$. The period of the carrier wave is 16 s, and the period of the envelope is 5994 s. The carrier wave frequency is $\omega = 0.39$ s^{-1}; the wavenumber k is obtained implicitly from (3) for the depth variation given in (59) using (60), (61), and $g = 9.8$ m/s^2.

The results shown in Fig. 6 are in the physical time frame, T, and are calculated for

$\hat{\epsilon} = 0.1$ and $D = 599.4$ s (see Table II). The period D corresponds to the time scale, τ, which is related to the physical time, T, according to (2b). From (2b), one may see that the time period corresponding to the scale T is equal to the time period corresponding to τ divided by $\hat{\epsilon}$. Therefore, the amplitude-envelopes shown in Fig. 6 have a period of $599.4/0.1 = 5994$ s. The black (solid and dotted) curves in Fig. 6 represent the amplitude envelopes and the grey curves represent the wave group whose period is 16 s. These grey curves cannot be distinguished because there are about 375 carrier wave periods for each envelope period.

V. SUMMARY

In this paper, we have analyzed narrow-banded, periodic one-dimensional surface gravity waves propagating on water of variable depth. We obtained the general forms of five Jacobi-elliptic functions that are approximate solutions of the DRE. For each of the five cases, we obtained the maximum envelope-amplitude and the envelope-width as functions of the distance of propagation. For all five cases the maximum envelope-amplitude decreased with decreasing depth, while the envelope-width increased with decreasing depth. The largest decrease in the maximum envelope-amplitude and correspondingly the largest increase in the envelope-width over the interval of propagation were observed for case #5, in which the envelope of the carrier wave was described using a combination of the Jacobi-dn and Jacobi-nd functions. The smallest decrease in the maximum envelope-amplitude and correspondingly the smallest increase in the envelope-width over the interval of propagation were observed for case #4, in which the envelope of the carrier wave was described using the Jacobi-sd function. In the limit of the elliptic modulus, m, approaching one, three of the five solutions: the Jacobi-cn solution, the Jacobi-nd solution, and the solution which is a combination of both the Jacobi-dn and Jacobi-nd functions, reduce to the soliton solution analyzed in Benilov, Flanagan, and Howlin[5]. In the limit of the elliptic modulus, m, approaching zero, two of the five solutions: the Jacobi-dn solution, and the Jacobi-nd solution, reduce to the uniform (in τ) envelope-amplitude solution (analyzed in Rajan[2], Chapter 2, pp 15-32), whose envelope-amplitude also decreases with decreasing depth.

Acknowledgements

We are grateful for helpful discussions with David Sandwell and Walter Munk. This work was supported by the National Science Foundation NSF-DMS 1107379. Bayram thanks

AWM-NSF for funding her expenses to travel and collaborate with Henderson at Penn State University during and after Summer 2010 with an AWM-NSF Mentoring Travel Grant Award.

Appendix A: Equations for Uniform Depth

If the bathymetry is uniform, the coefficients α and β become constants, and $\mu \equiv 0$, so that (11) reduces to

$$\mathrm{i}\epsilon\frac{\partial A}{\partial \xi} + \alpha\frac{\partial^2 A}{\partial \tau^2} + \beta|A|^2 A = 0. \tag{A1}$$

Following Carter and Segur[14], we assume a solution to (A1) of the form

$$A(\xi,\tau) = A_0\ f(\lambda\tau)\ \exp\{\mathrm{i}c_2\xi\}, \tag{A2}$$

where

$$A_0 = |A_0|\ \exp(\mathrm{i}\varphi). \tag{A3}$$

Substituting (A2) and (A3) in (A1), we obtain

$$-\epsilon f c_2 + \alpha\lambda^2 f'' + \beta|A_0|^2 f^3 = 0, \tag{A4}$$

which yields

$$f'' = \frac{\epsilon c_2}{\alpha\lambda^2} f - \frac{\beta|A_0|^2}{\alpha\lambda^2} f^3, \tag{A5}$$

where $f' = \mathrm{d}f/\mathrm{d}(\lambda\tau)$. Integrating (A5) once, we obtain

$$(f')^2 = \frac{\epsilon c_2}{\alpha\lambda^2} f^2 - \frac{\beta|A_0|^2}{2\alpha\lambda^2} f^4 + c_3. \tag{A6}$$

Since $kh > 1.363$ and $\beta/\alpha > 0$ in this analysis, it follows that

$$\frac{\epsilon c_2}{\alpha\lambda^2} \lessgtr 0, \tag{A7a}$$

$$\frac{\beta|A_0|^2}{2\alpha\lambda^2} > 0, \tag{A7b}$$

in (A6). Equation (A6) can be compared to the nonlinear differential equations appropriate for various Jacobi-elliptic functions listed in Table III.

We compare the coefficient of f^4 in (A6) with the coefficient of Y^4 in Table III. Based on the conditions in (A7), we note that there are four possible Jacobi-elliptic function solutions

that satisfy (A6), namely the cn, dn, nd, and sd functions. The structure of (A5) suggests an additional solution of the form $f \sim a(m)\mathrm{nd}(\lambda\tau; m) + b(m)\mathrm{dn}(\lambda\tau; m)$, where a and b are appropriate functions of m. Consequently, it turns out that

$$Y = \sqrt{1-m^2}\ \mathrm{nd}(\lambda\tau; m) + \mathrm{dn}(\lambda\tau; m) \tag{A8}$$

satisfies the nonlinear equation

$$Y'' = \left[2 + 6\sqrt{1-m^2} - m^2\right] Y - 2Y^3, \tag{A9}$$

where $Y' = \mathrm{d}Y/\mathrm{d}(\lambda\tau)$. Therefore, there are five exact solutions of (A5), namely,

1. $f = \mathrm{cn}(\lambda\tau; m)$,
2. $f = \mathrm{dn}(\lambda\tau; m)$,
3. $f = \mathrm{nd}(\lambda\tau; m)$,
4. $f = \mathrm{sd}(\lambda\tau; m)$, and

TABLE III. Differential equations for various Jacobi-elliptic functions (*e.g.*, Olver *et al.*[15], Chapter 22). For all cases, $0 \leqslant m \leqslant 1$. $Y' = \mathrm{d}Y/\mathrm{d}(\lambda\tau)$.

Function	Differential Equation
$Y = \mathrm{sn}, \mathrm{cd}$	$(Y')^2 = 1 - (1+m^2)Y^2 + m^2Y^4$
$Y = \mathrm{cn}$	$(Y')^2 = (1-m^2) + (2m^2-1)Y^2 - m^2Y^4$
$Y = \mathrm{dn}$	$(Y')^2 = (m^2-1) + (2-m^2)Y^2 - Y^4$
$Y = \mathrm{ns}, \mathrm{dc}$	$(Y')^2 = m^2 - (1+m^2)Y^2 + Y^4$
$Y = \mathrm{nc}$	$(Y')^2 = -m^2 + (2m^2-1)Y^2 + (1-m^2)Y^4$
$Y = \mathrm{nd}$	$(Y')^2 = -1 + (2-m^2)Y^2 - (1-m^2)Y^4$
$Y = \mathrm{sc}$	$(Y')^2 = 1 + (2-m^2)Y^2 + (1-m^2)Y^4$
$Y = \mathrm{sd}$	$(Y')^2 = 1 + (2m^2-1)Y^2 - m^2(1-m^2)Y^4$
$Y = \mathrm{cs}$	$(Y')^2 = (1-m^2) + (2-m^2)Y^2 + Y^4$
$Y = \mathrm{ds}$	$(Y')^2 = -m^2(1-m^2) + (2m^2-1)Y^2 + Y^4$

TABLE IV. The constants c_2 and $|A_0|$ in (A5) and (A6).

#	f or J	c_2	$\lvert A_0\rvert$
1	$\mathrm{cn}(\lambda\tau;m)$	$\frac{1}{\epsilon}\Big[\big(2m^2-1\big)\alpha\lambda^2\Big]$	$m\lambda\sqrt{\frac{2\alpha}{\beta}}$
2	$\mathrm{dn}(\lambda\tau;m)$	$\frac{1}{\epsilon}\Big[\big(2-m^2\big)\alpha\lambda^2\Big]$	$\lambda\sqrt{\frac{2\alpha}{\beta}}$
3	$\mathrm{nd}(\lambda\tau;m)$	$\frac{1}{\epsilon}\Big[\big(2-m^2\big)\alpha\lambda^2\Big]$	$\lambda\sqrt{\frac{2\alpha(1-m^2)}{\beta}}$
4	$\mathrm{sd}(\lambda\tau;m)$	$\frac{1}{\epsilon}\Big[\big(2m^2-1\big)\alpha\lambda^2\Big]$	$m\lambda\sqrt{\frac{2\alpha(1-m^2)}{\beta}}$
5	$\sqrt{1-m^2}\ \mathrm{nd}(\lambda\tau;m)+\mathrm{dn}(\lambda\tau;m)$	$\frac{1}{\epsilon}\Big[\Big(2+6\sqrt{1-m^2}-m^2\Big)\alpha\lambda^2\Big]$	$\lambda\sqrt{\frac{2\alpha}{\beta}}$

5. $f=\sqrt{1-m^2}\ \mathrm{nd}(\lambda\tau;m)+\mathrm{dn}(\lambda\tau;m)$.

Comparing (A6) with the differential equations (listed in Table III) satisfied by these five functions, we obtain the values of the constants c_2 and $|A_0|$; they are listed in Table IV. From (A2) and (A3), we obtain

$$A(\xi,\tau)=|A_0|\ J(\lambda\tau;m)\ \exp\big[\mathrm{i}c_2\xi\big]\ \exp(\mathrm{i}\varphi), \tag{A10}$$

where $J(\lambda\tau;m)$, $|A_0|$, and c_2 correspond to one of the five cases in Table IV. For cases 1, 2 and 5 of Table IV, we obtain the soliton (sech) solution in the limit $m\to 1$,

$$A(\xi,\tau)=\lambda\sqrt{\frac{2\alpha}{\beta}}\ \mathrm{sech}(\lambda\tau)\ \exp\Big[\mathrm{i}\alpha\lambda^2\xi\Big]\ \exp(\mathrm{i}\varphi). \tag{A11}$$

We note that since (A10) and (A11) are for a uniform depth, the parameters λ, m, c_2, $|A_0|$, α, β are constants, as opposed to the case of variable depth, where all these parameters are spatially-varying, and thus functions of ξ.

REFERENCES

[1]V. D. Djordjević and L. G. Redekopp, Zeitschrift für Angewandte Mathematik und Physik (ZAMP) **29**, 950 (1978).

[2]G. K. Rajan, *Surface gravity waves propagating on water of finite, variable depth*, Master's thesis, The Pennsylvania State University, UP, USA (2012).

[3]R. Grimshaw, Journal of Fluid Mechanics **42**, 639 (1970).

[4]R. Grimshaw, Journal of Fluid Mechanics **46**, 611 (1971).

[5]E. S. Benilov, J. D. Flanagan, and C. P. Howlin, Journal of Fluid Mechanics **533**, 171 (2005).

[6]R. H. J. Grimshaw and S. Y. Annenkov, Studies in Applied Mathematics **126**, 409 (2011).

[7]T. B. Benjamin and J. E. Feir, Journal of Fluid Mechanics **27**, 417 (1967).

[8]P. A. E. M. Janssen and M. Onorato, Journal of Physical Oceanography **37**, 2389 (2007).

[9]H. Zeng and K. Trulsen, Natural Hazards and Earth System Sciences **12**, 631 (2012).

[10]K. Trulsen, H. Zeng, and O. Gramstad, Physics of Fluids **24**, 097101 (2012).

[11]O. Gramstad, H. Zeng, K. Trulsen, and G. K. Pedersen, Physics of Fluids **25**, 122103 (2013).

[12]P. F. Byrd and M. D. Friedman, *Handbook of Elliptic Integrals for Engineers and Physicists*, 2nd ed. (Springer, 1971).

[13]H. V. Thurman, *Introduction to oceanography 3rd edition* (Merril Publishing Company, 1981).

[14]J. D. Carter and H. Segur, Phys. Rev. E **68**, 045601 (2003).

[15]F. W. J. Olver, D. W. Lozier, R. F. Boisvert, and C. W. Clark, eds., *NIST Handbook of Mathematical Functions* (Cambridge University Press, New York, NY, 2010).

(a)

-0.5

-1

-1.5

$g\alpha$

0

5

10

15

20

kh

(b)

$\frac{2\beta g^3}{\omega^6}$

60
40
20
0
-20

0
5
10
15
20

kh

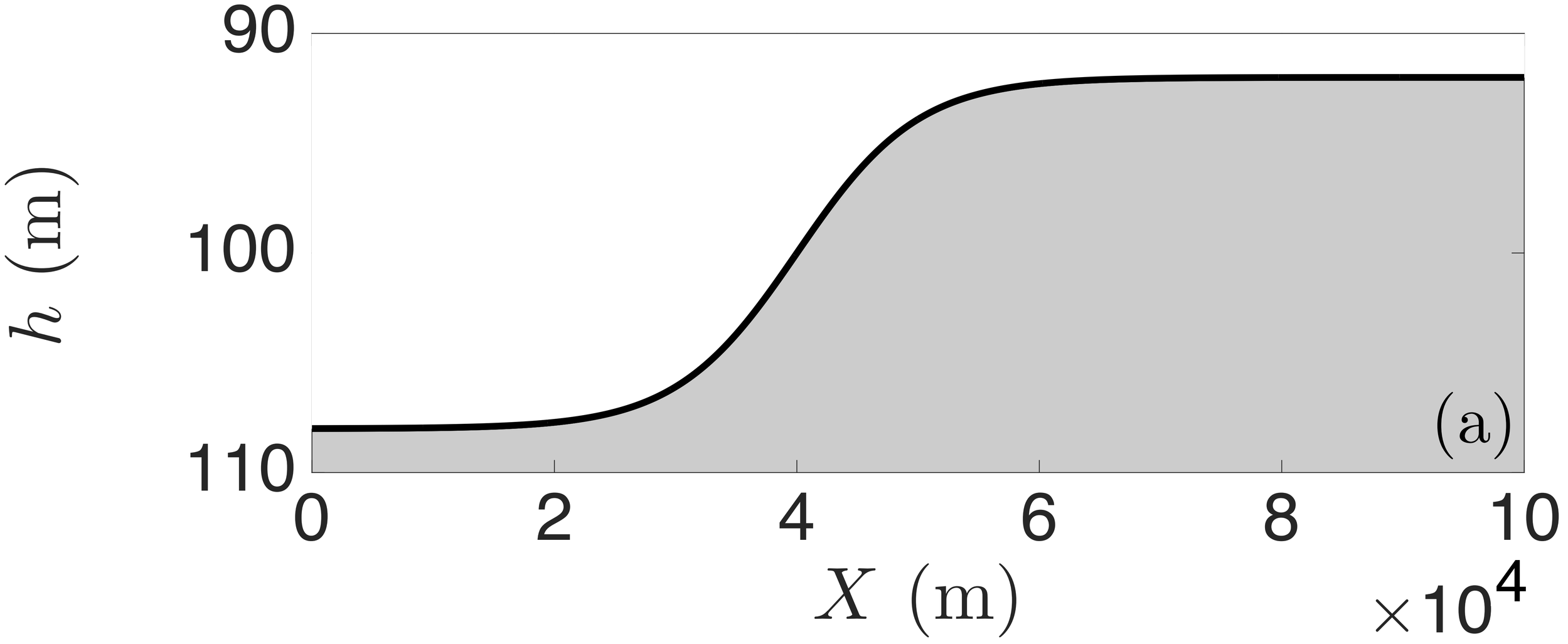

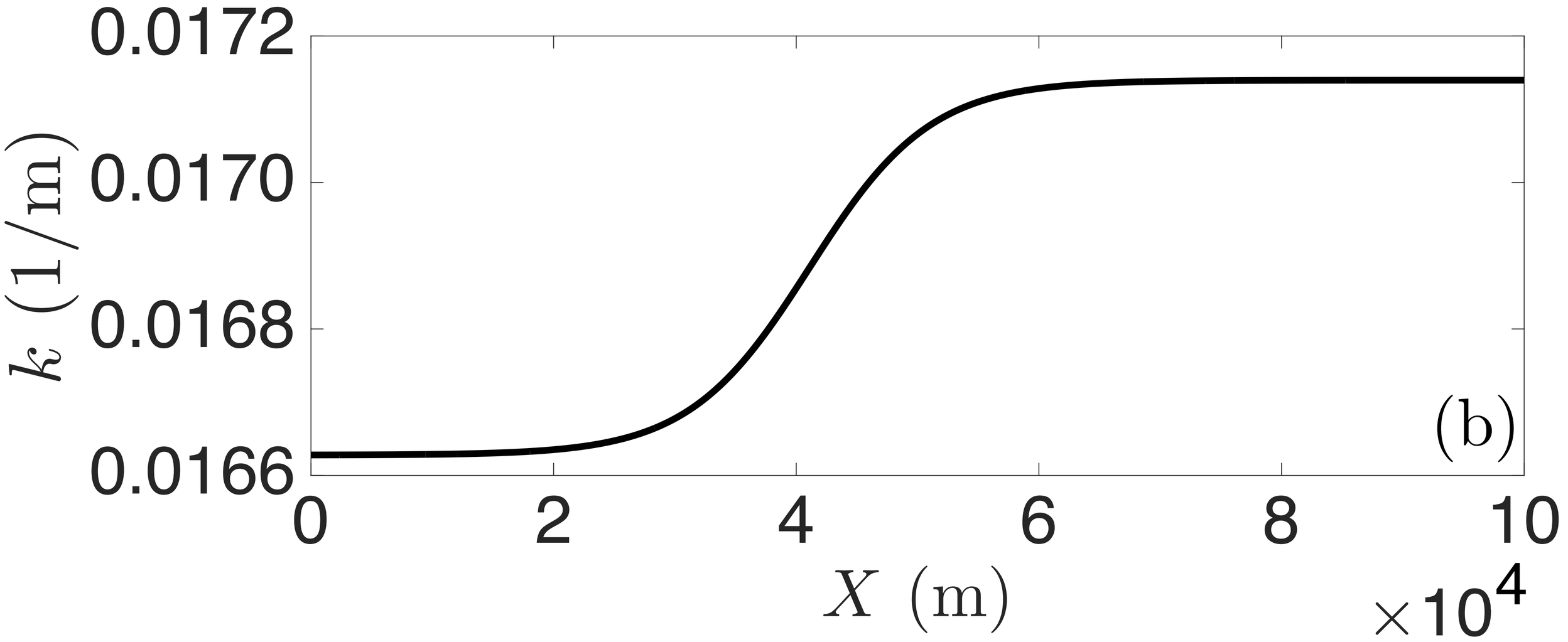

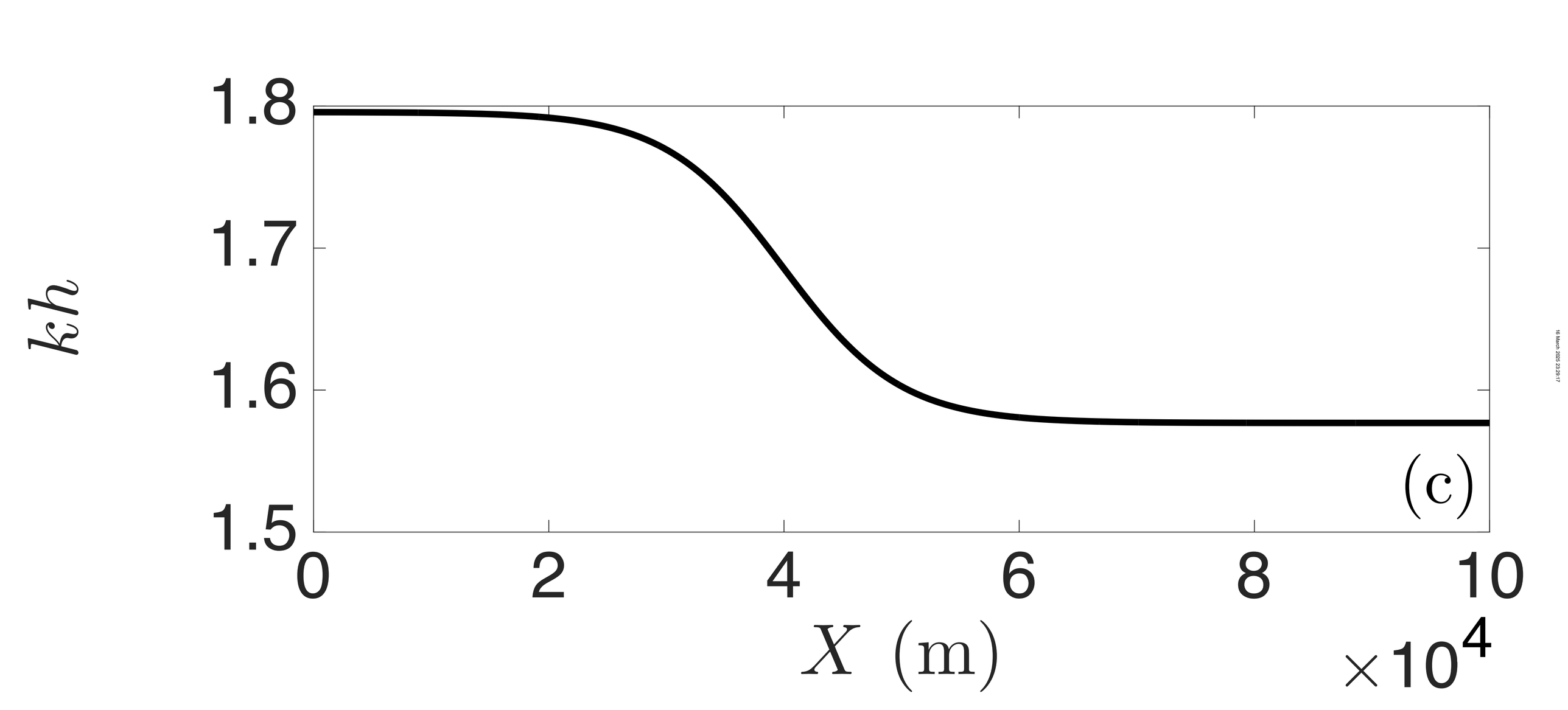

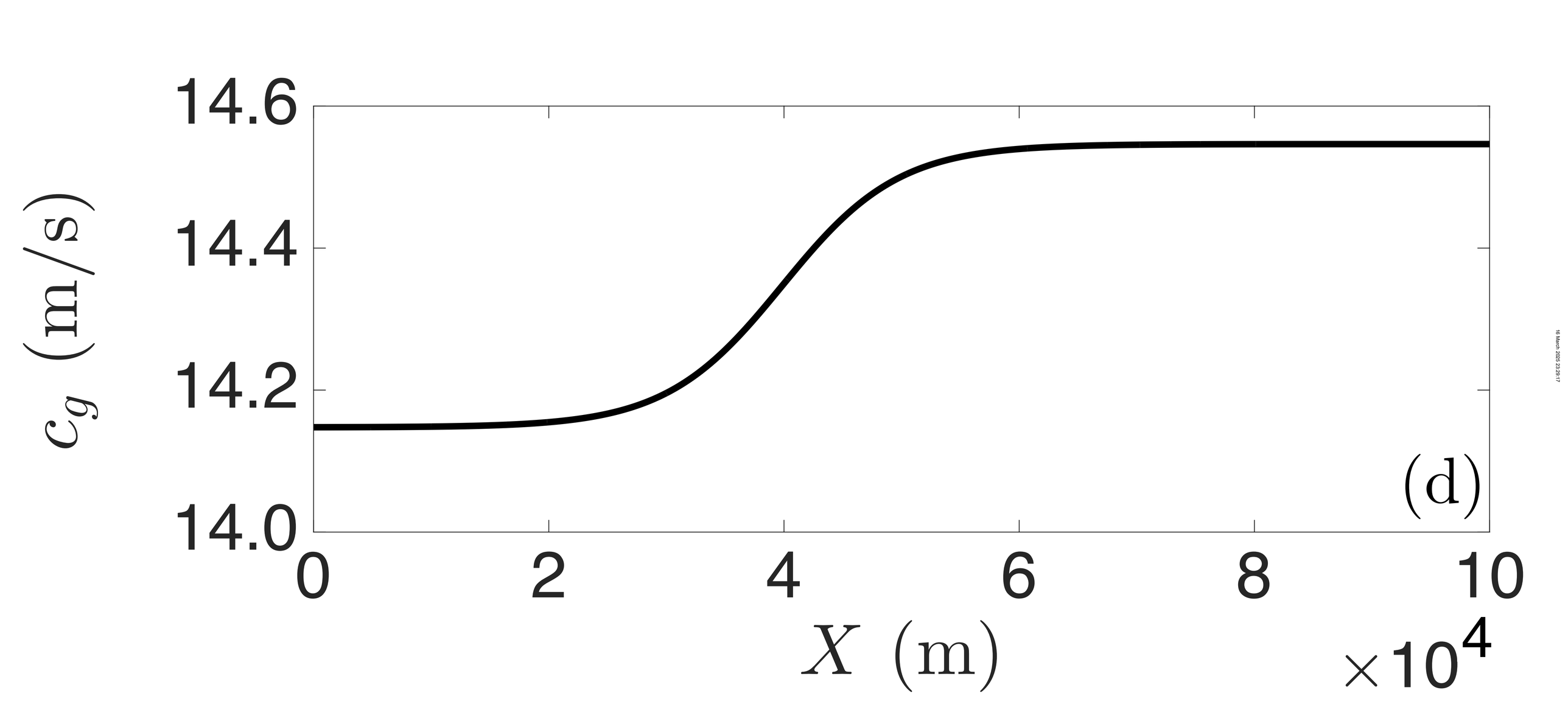

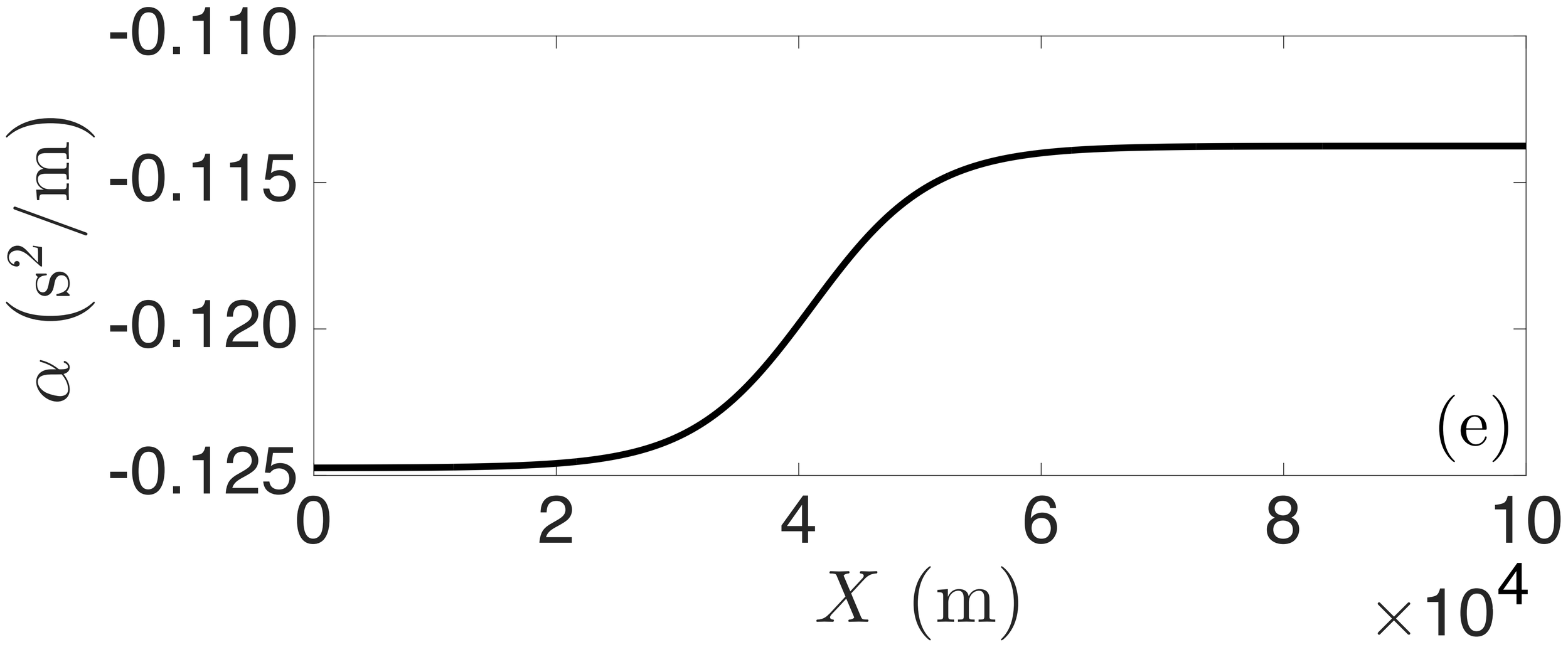

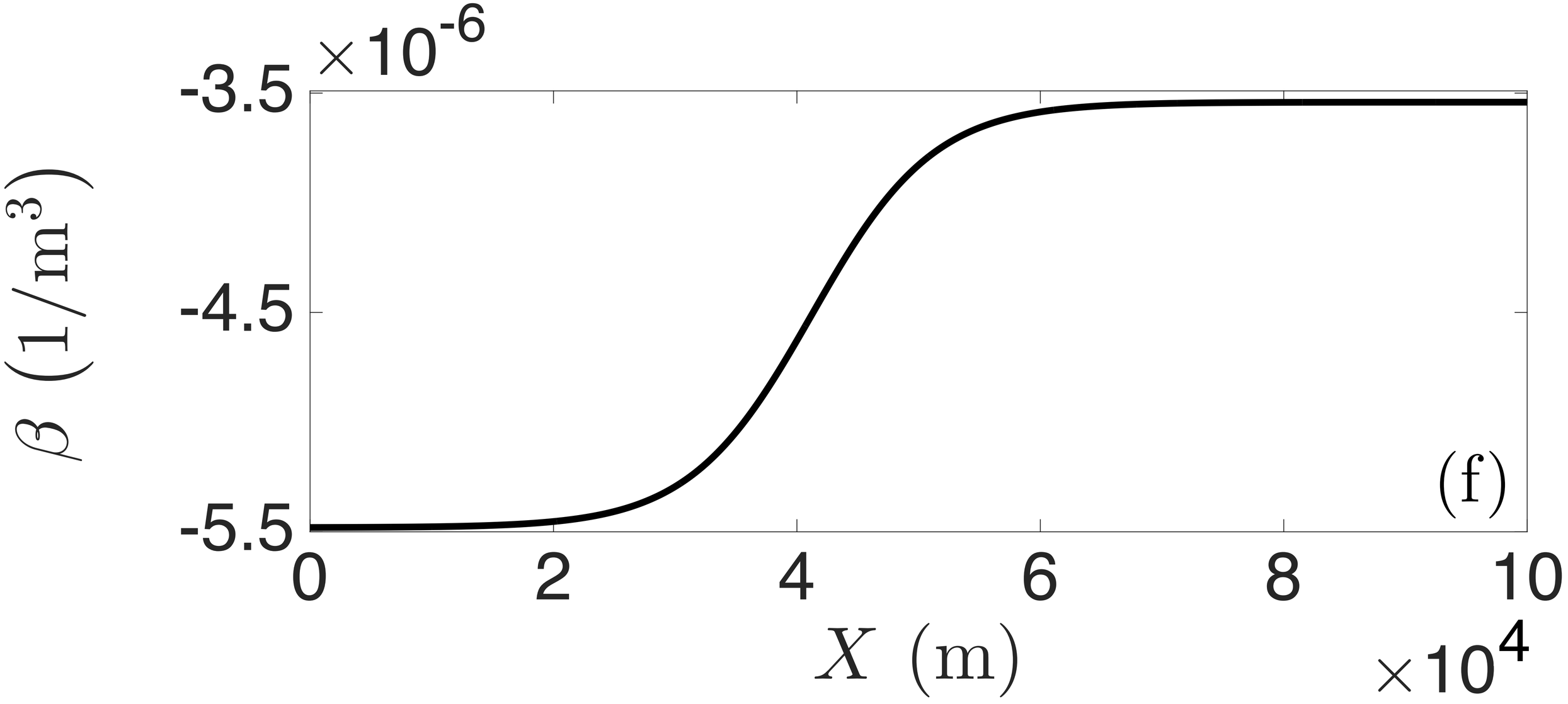
×10-6
-3.5
-4.5
-5.5
β (1/m3)
0
2
4
6
8
10
X (m)
×104
(f)

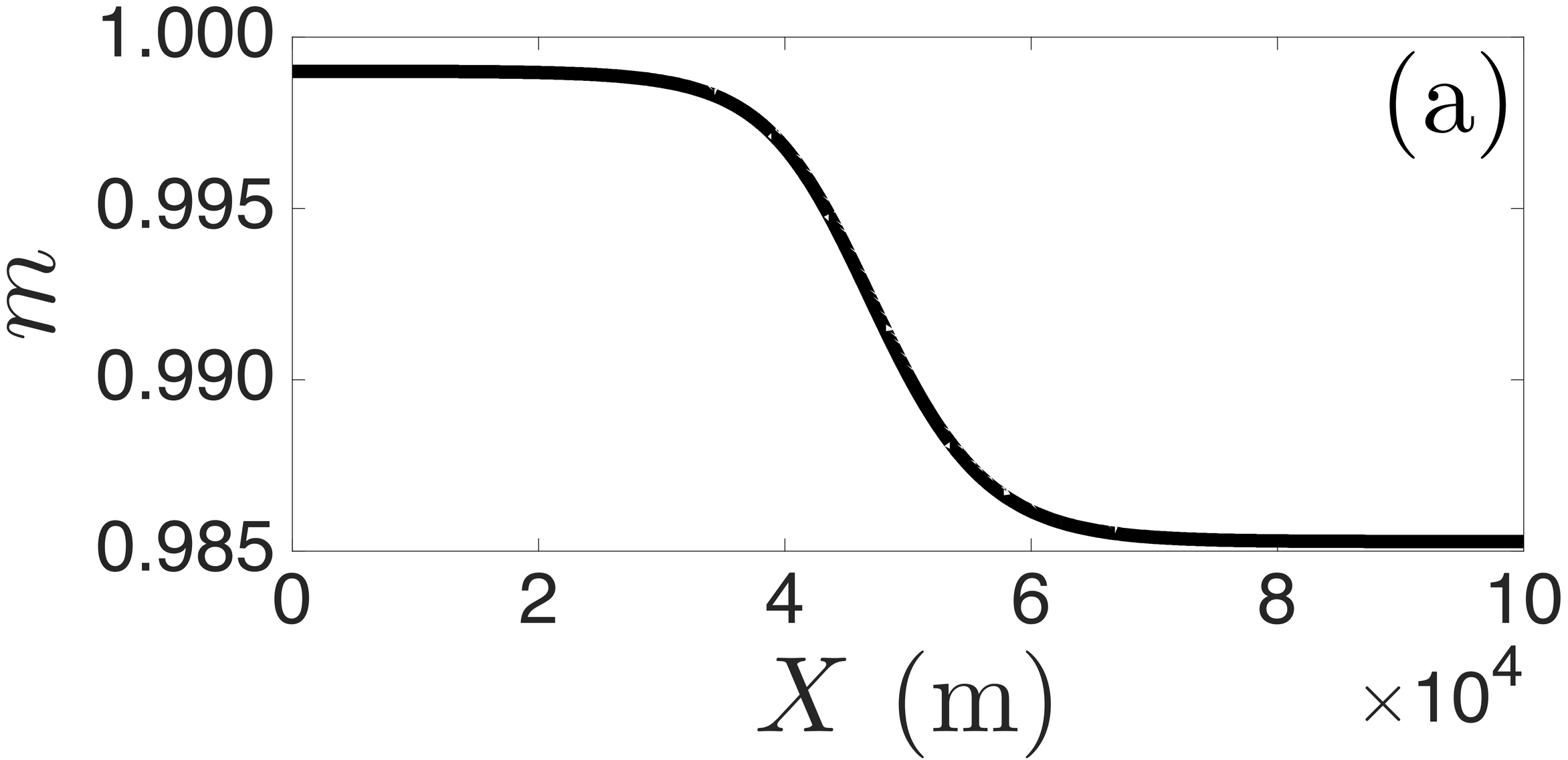

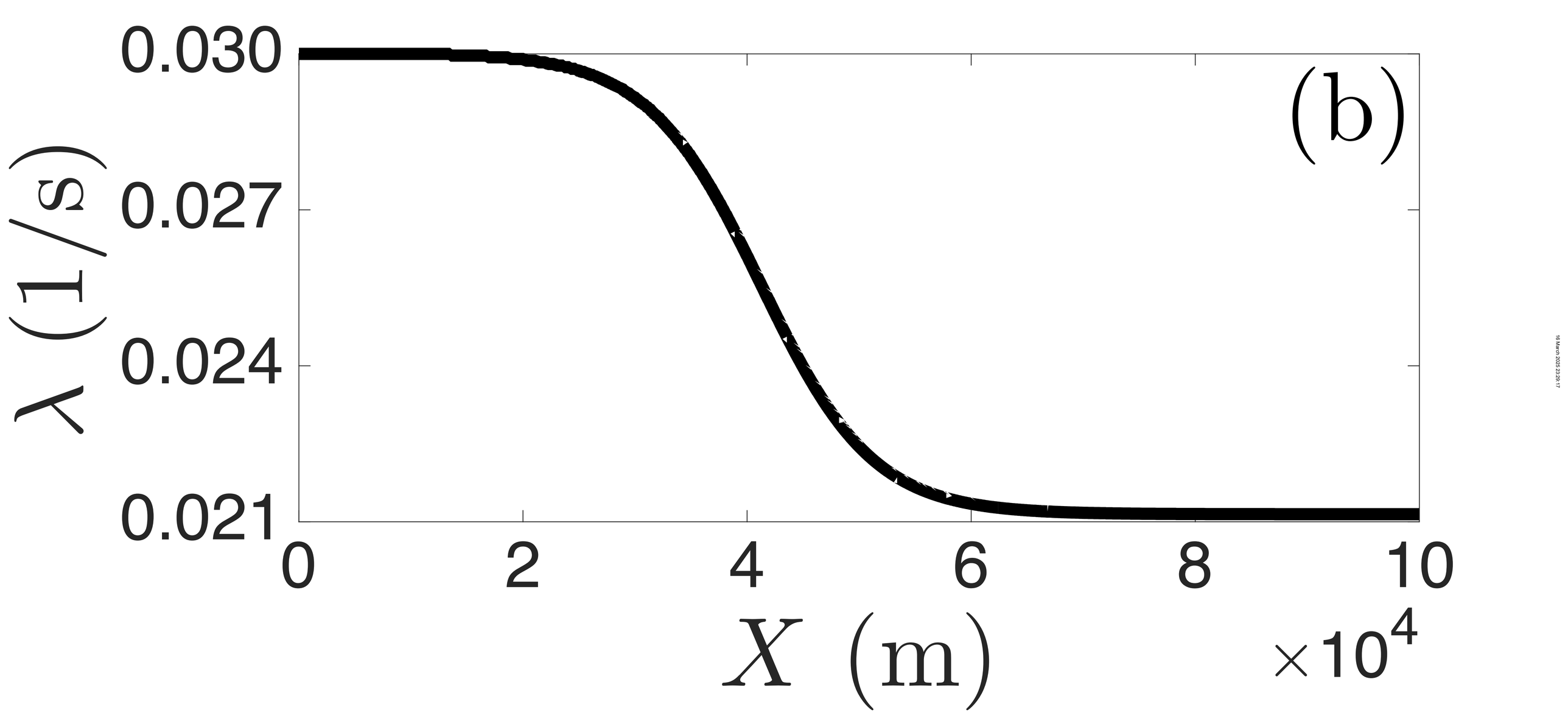
(b)
0.030
0.027
0.024
0.021
λ (1/s)
0
2
4
6
8
10
X (m)
×10^4

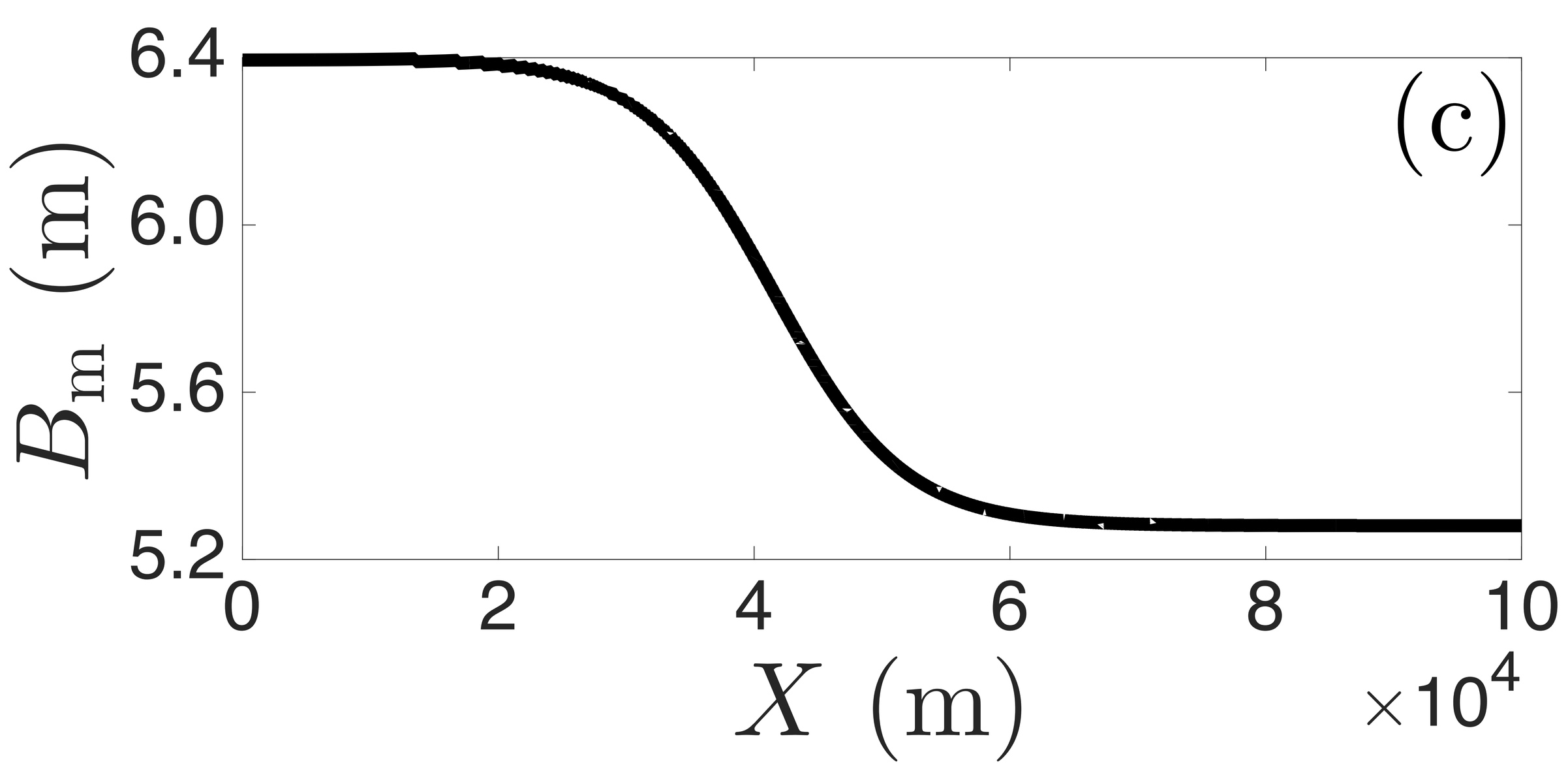

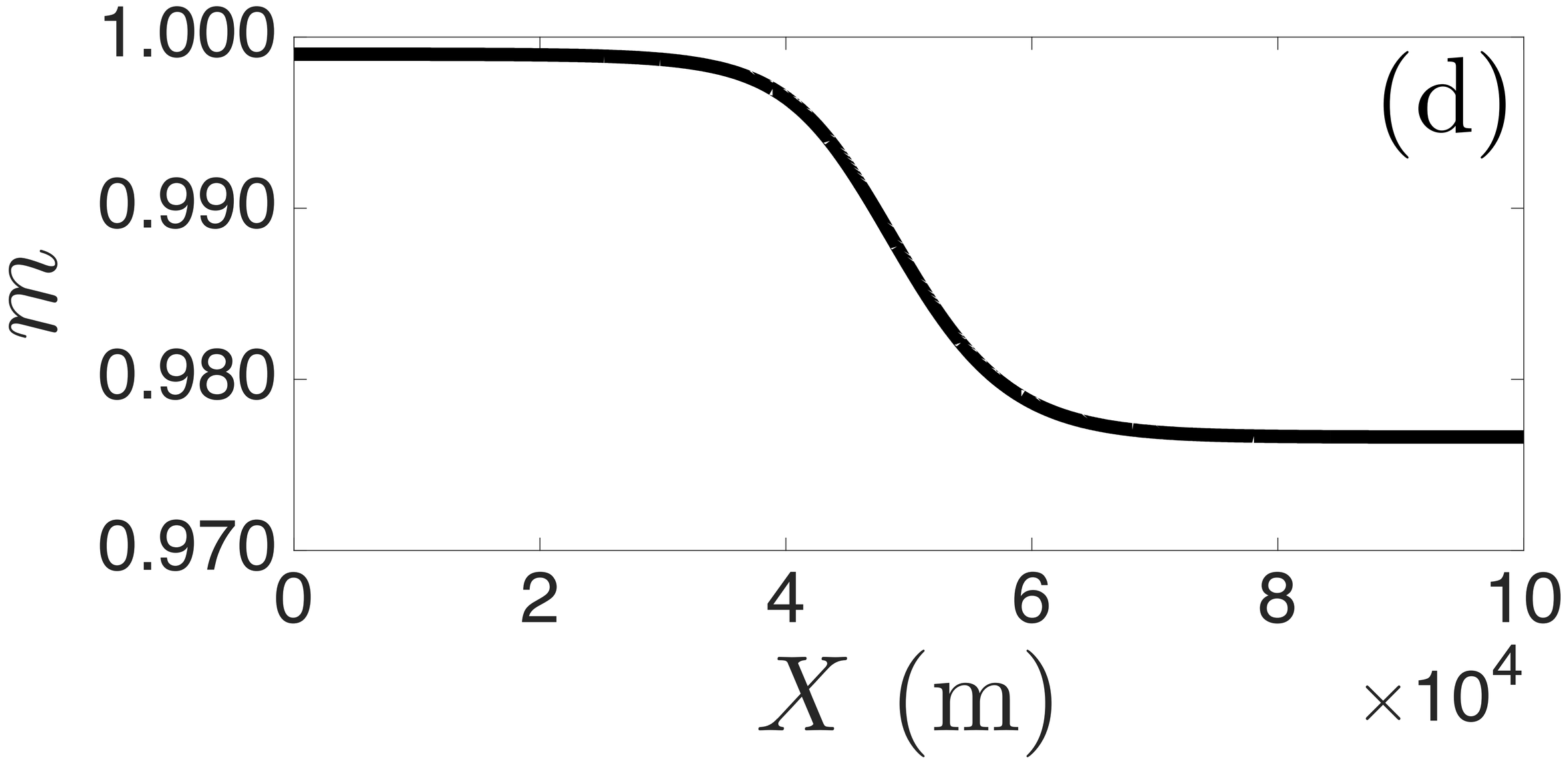

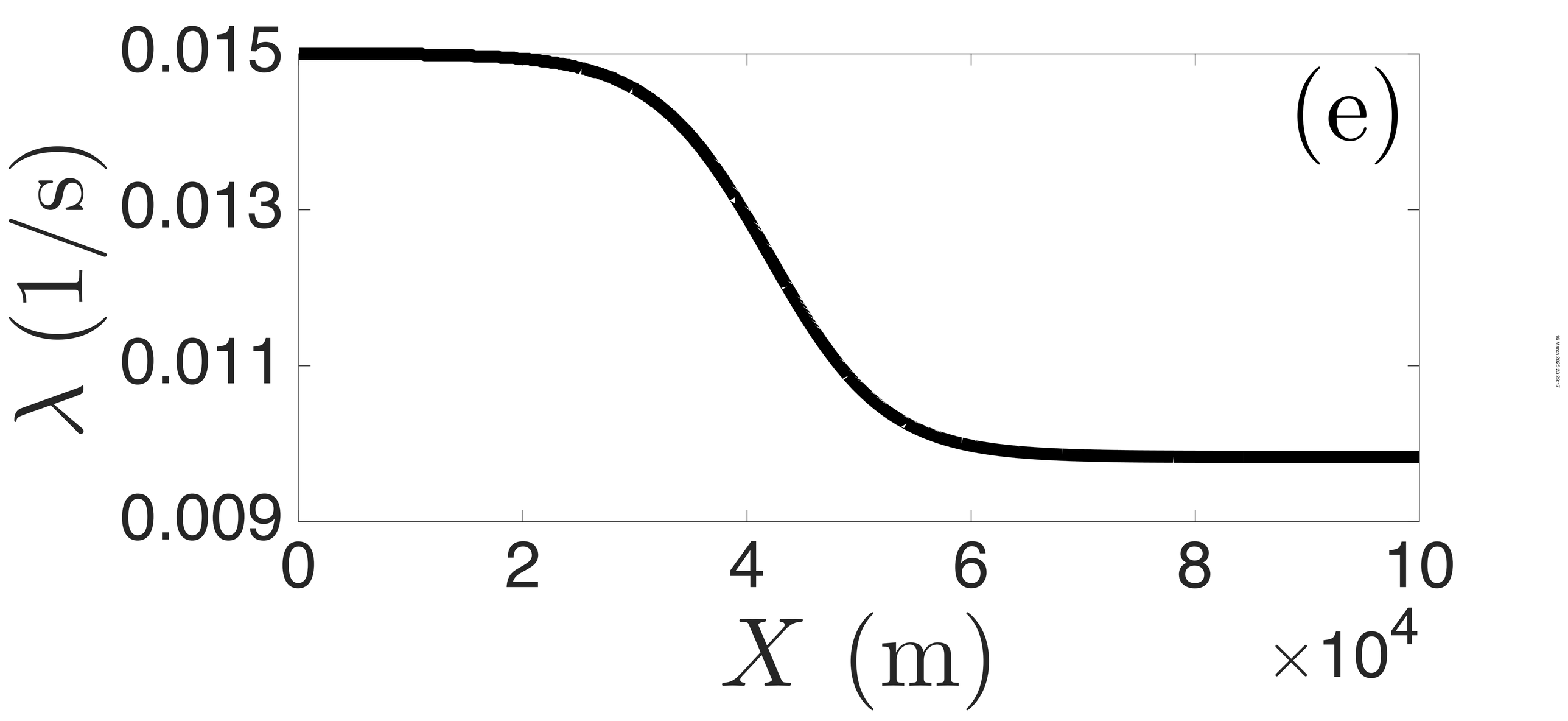

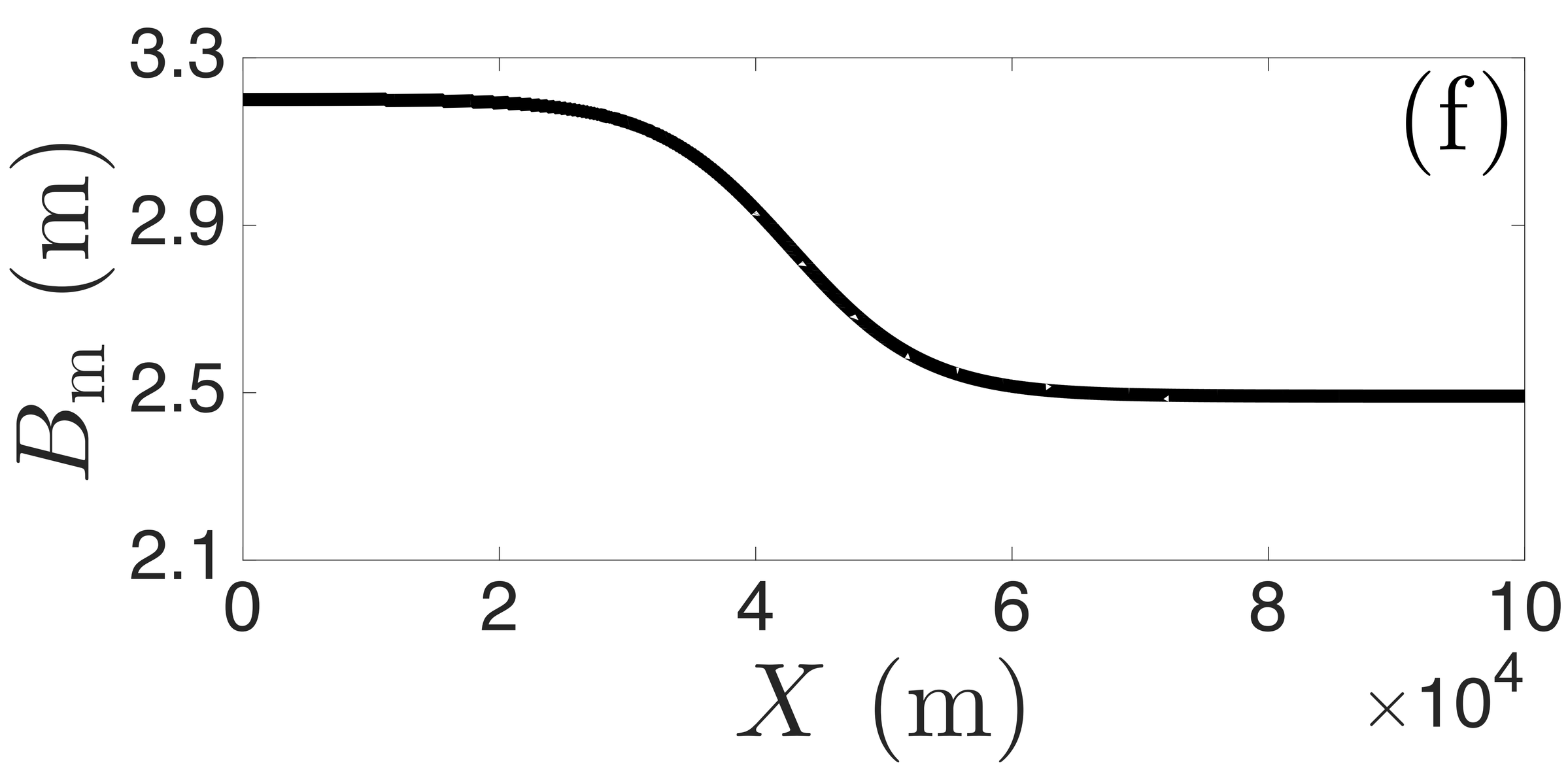

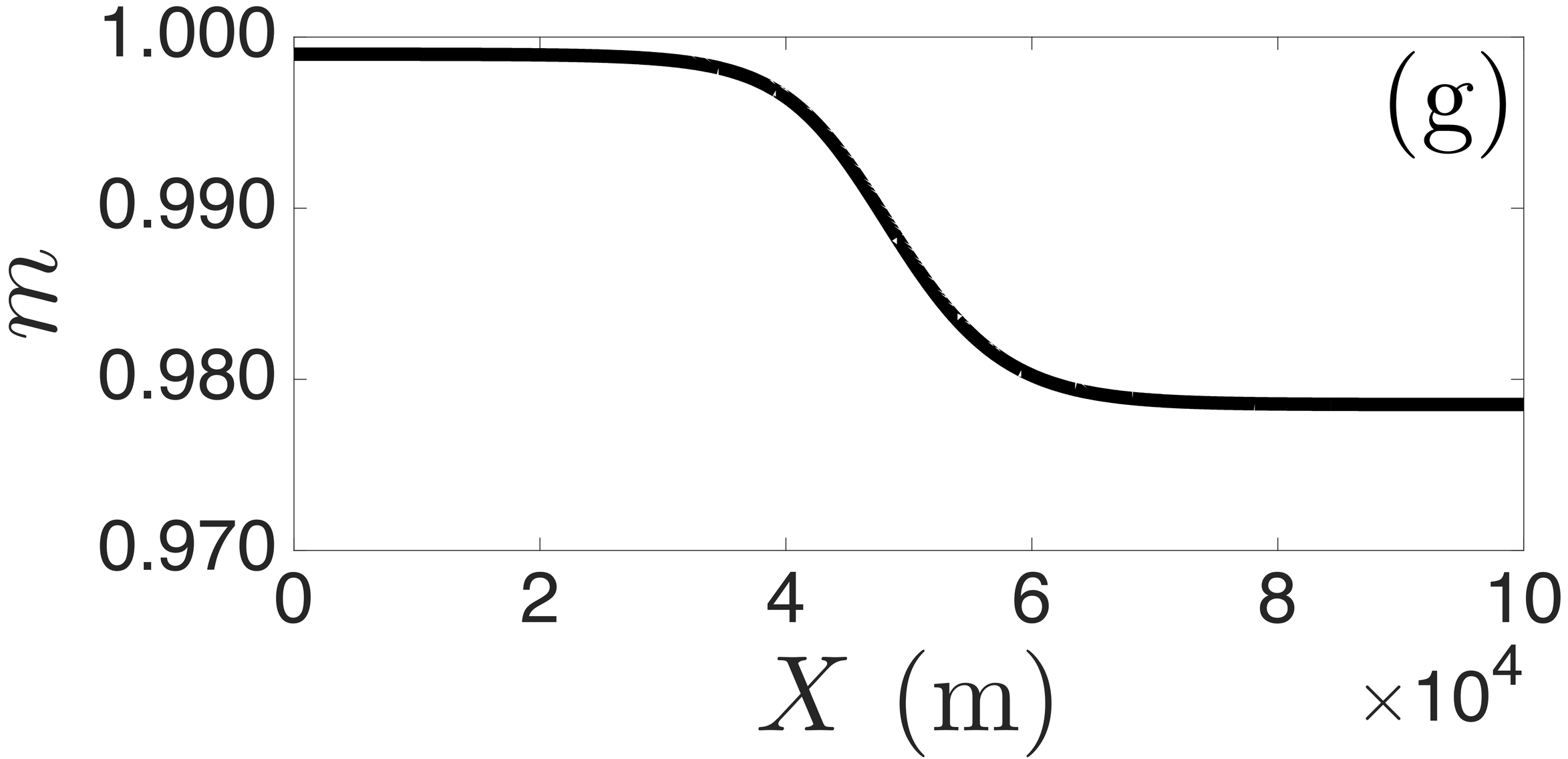

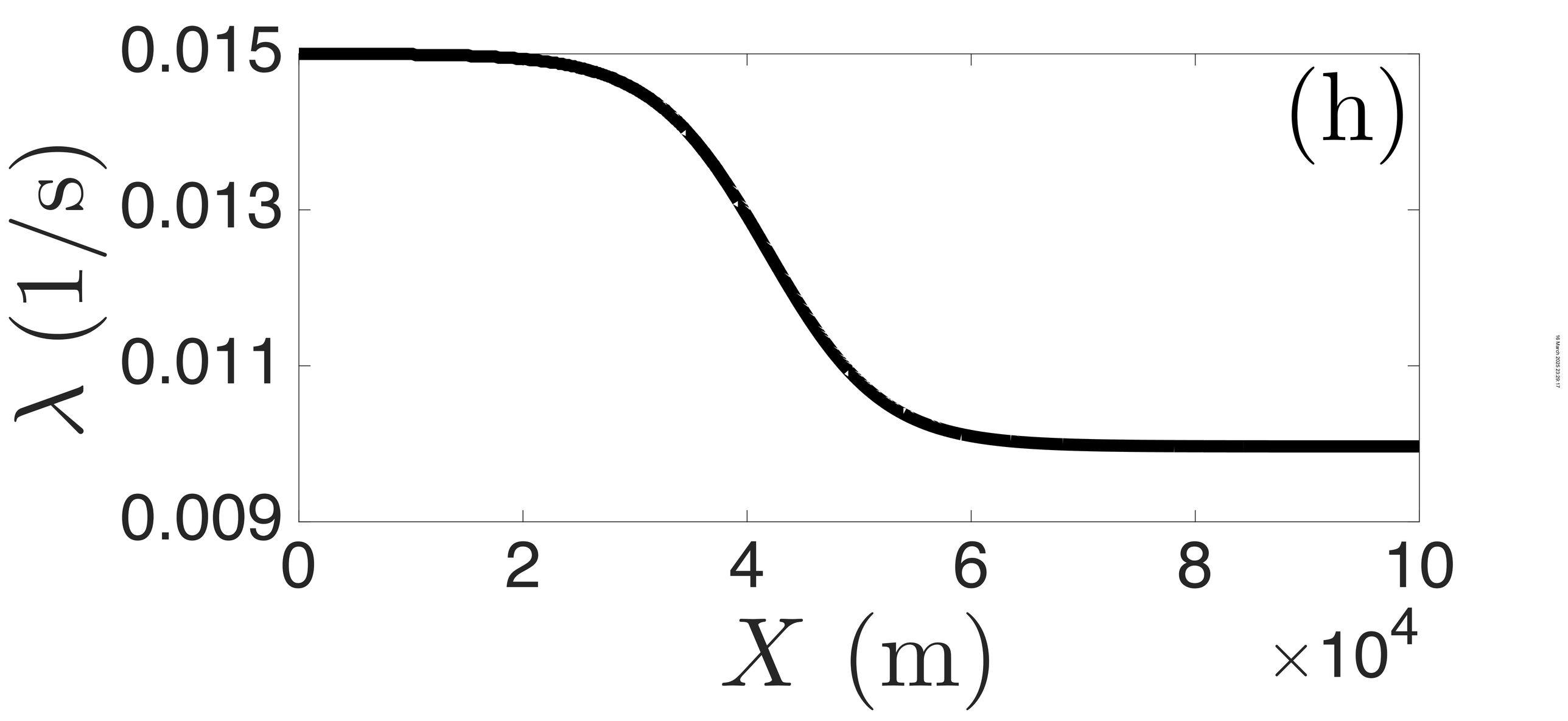

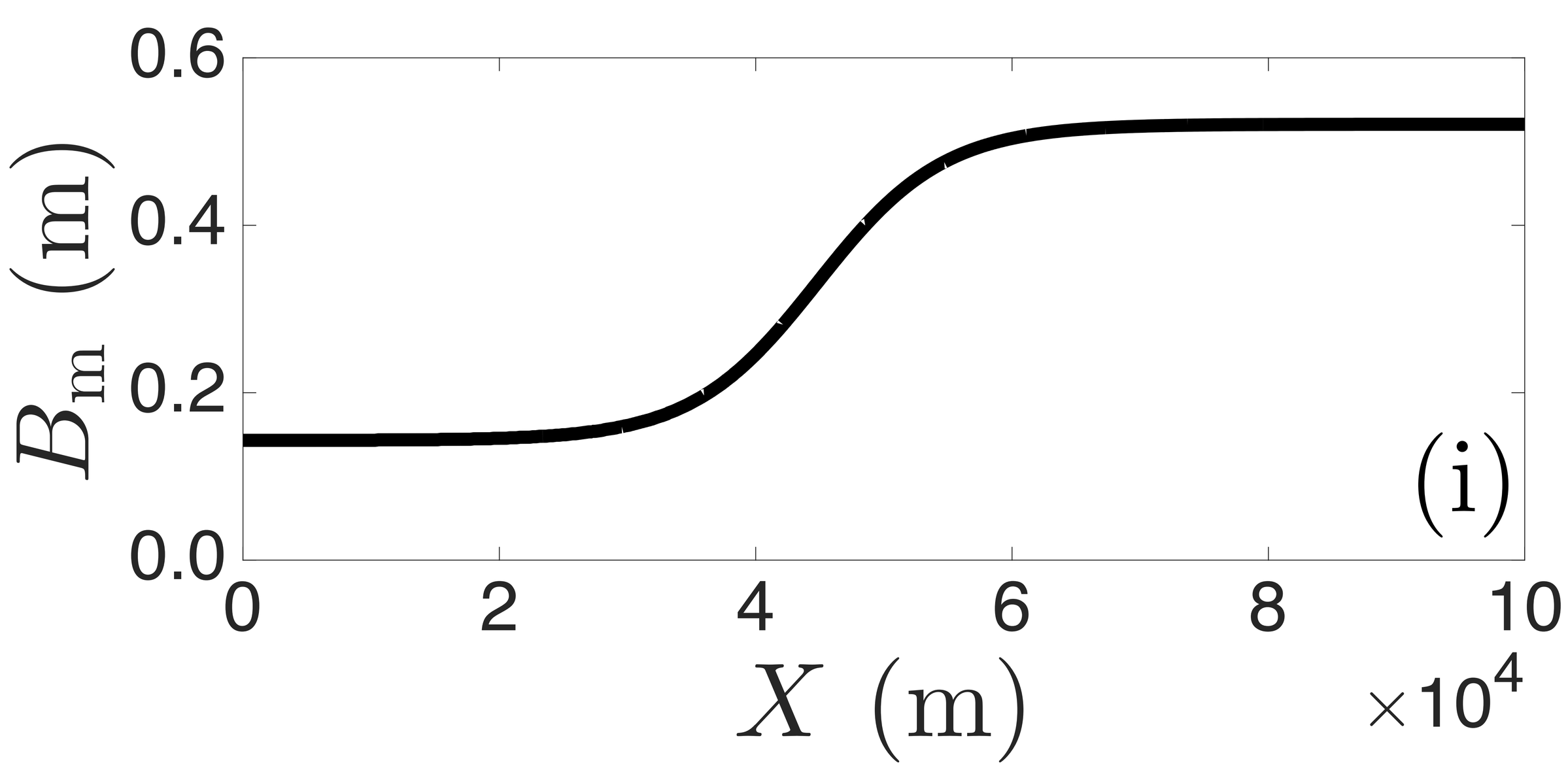

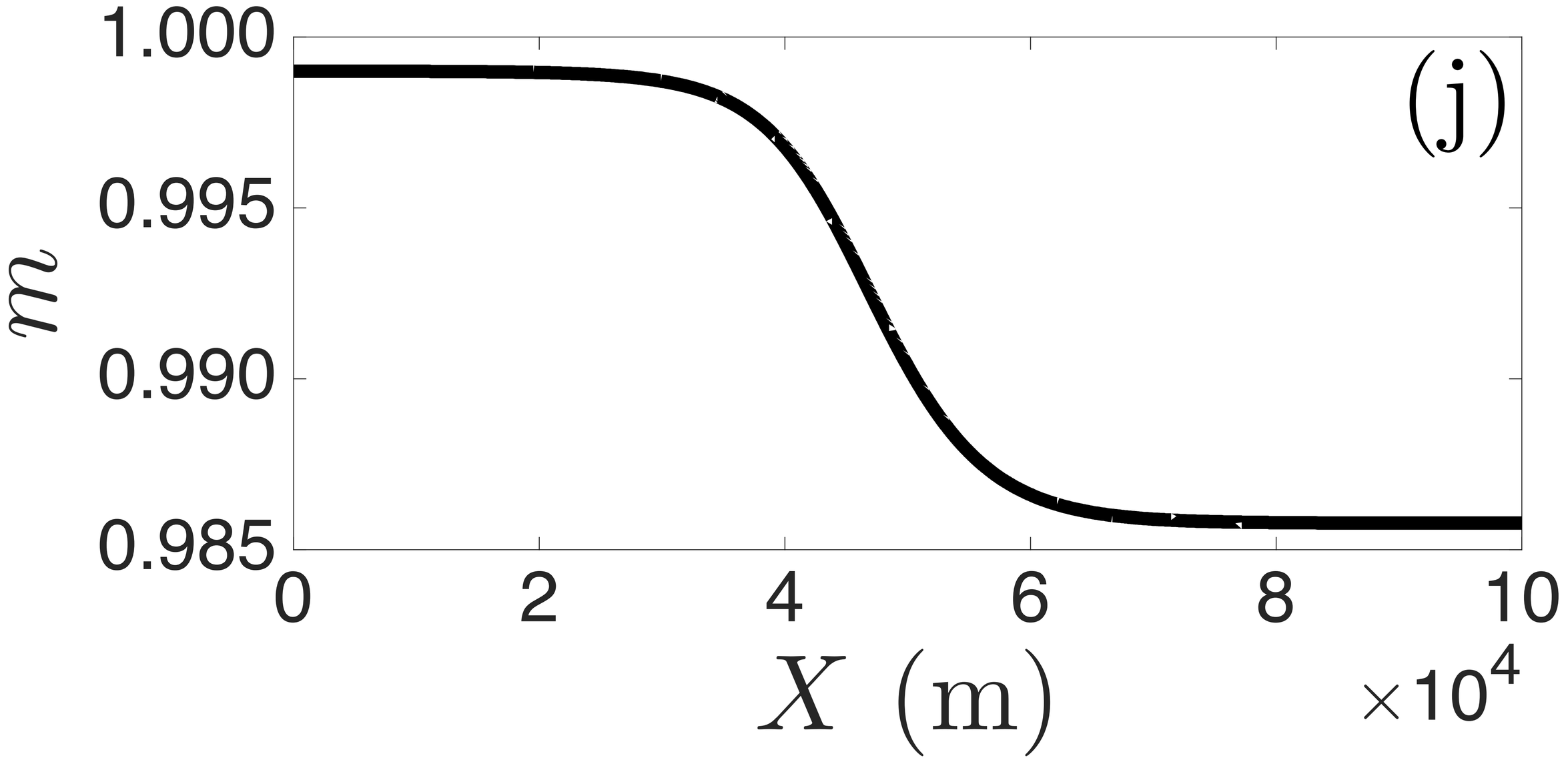

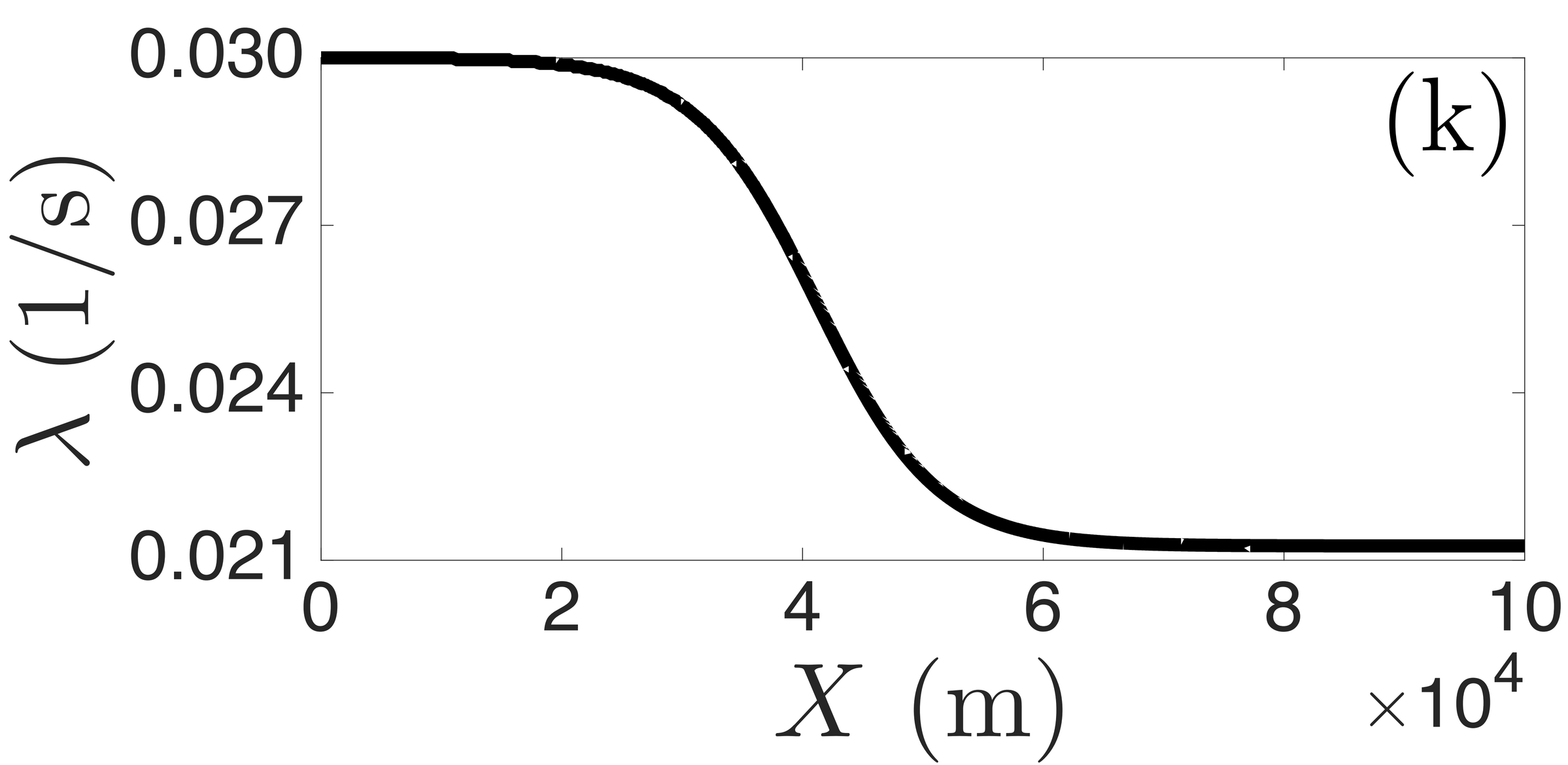

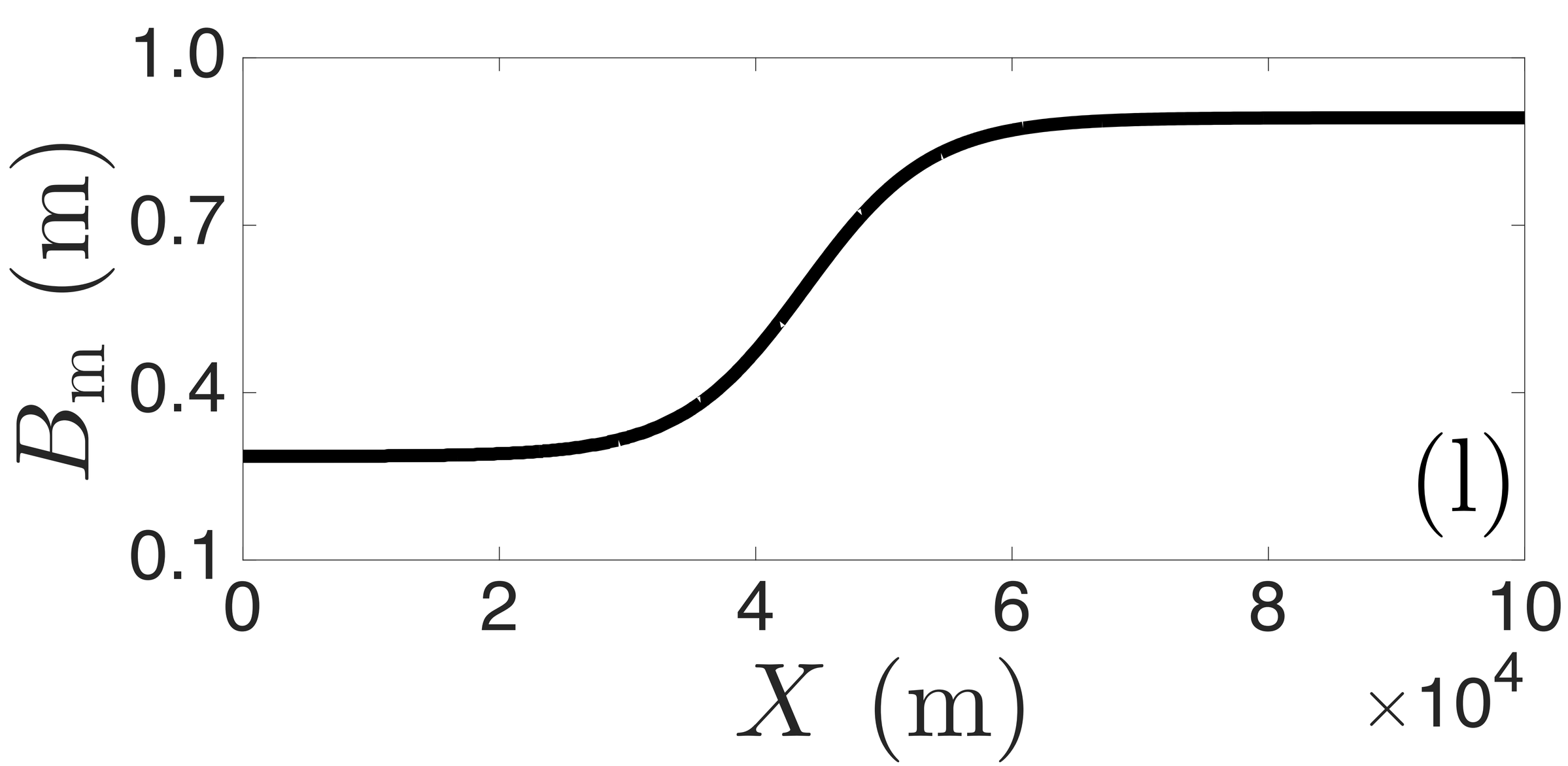

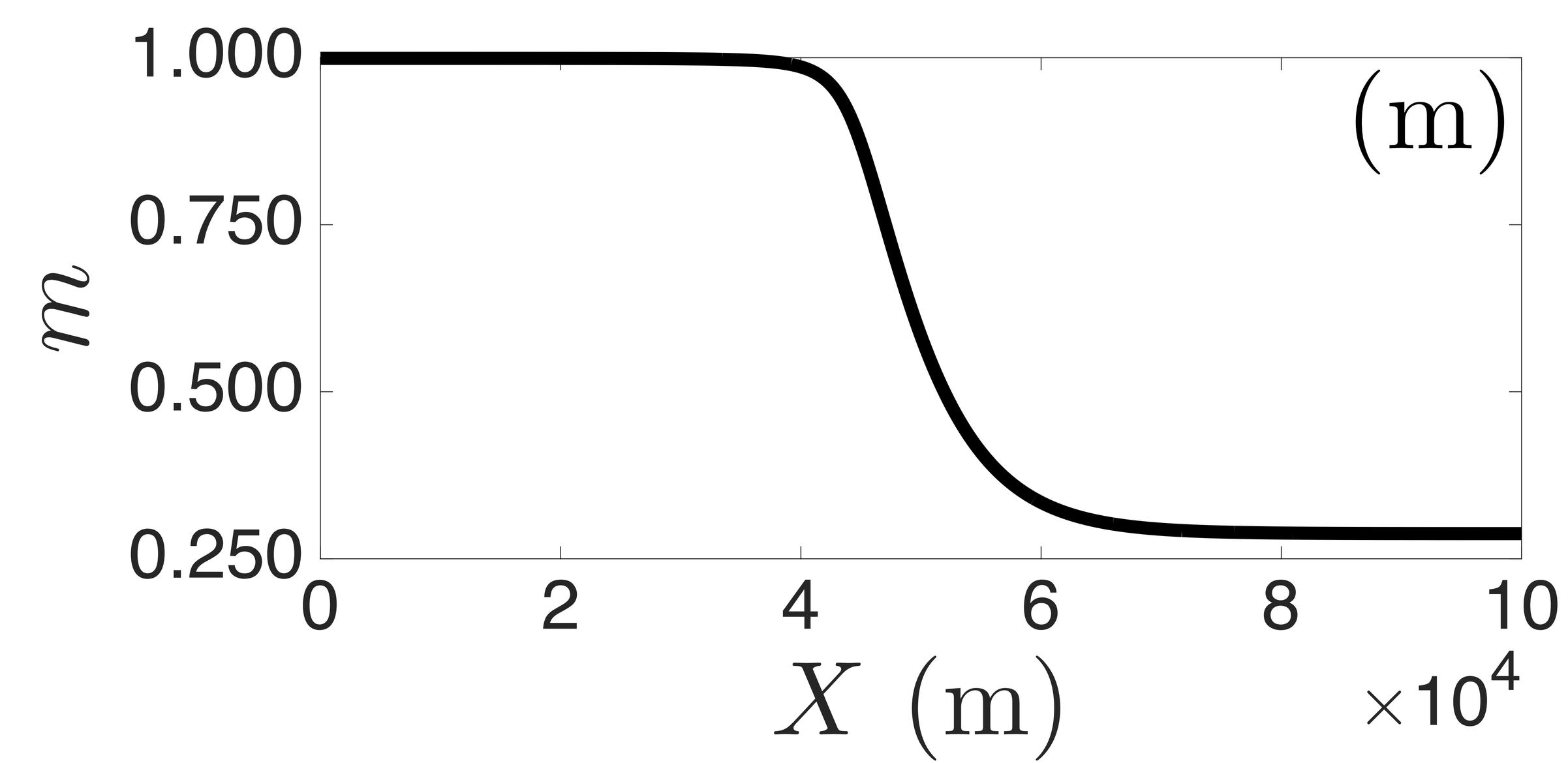

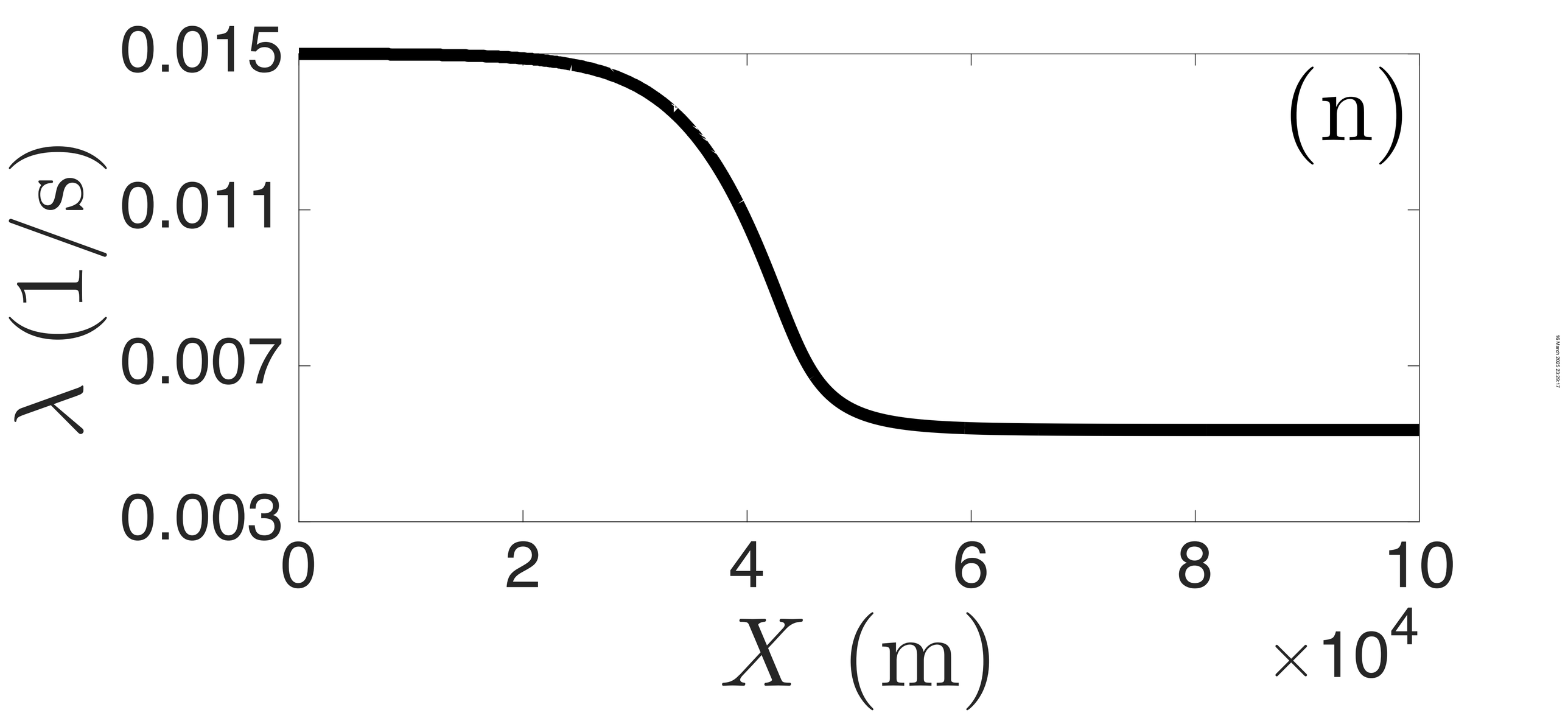

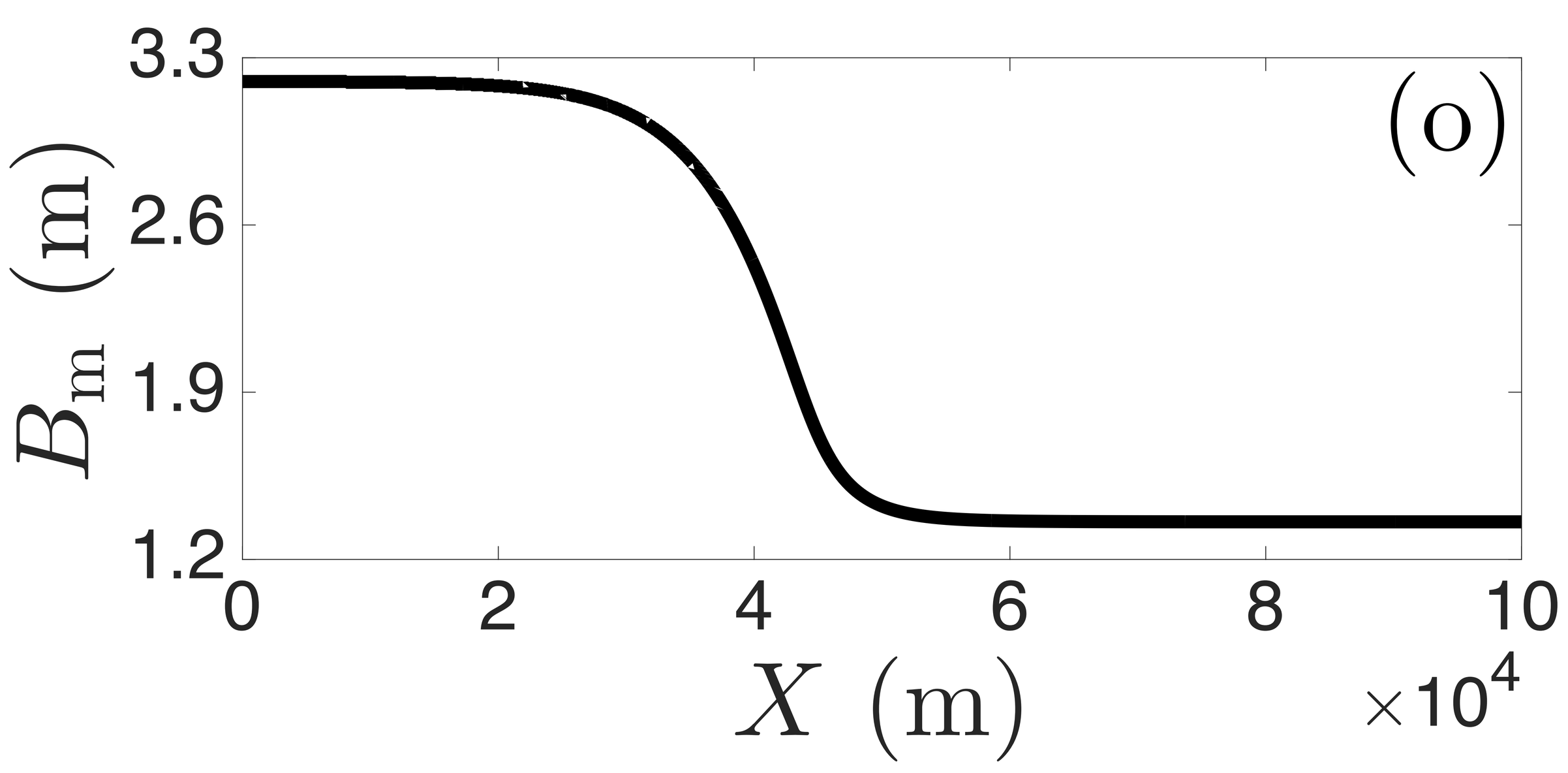

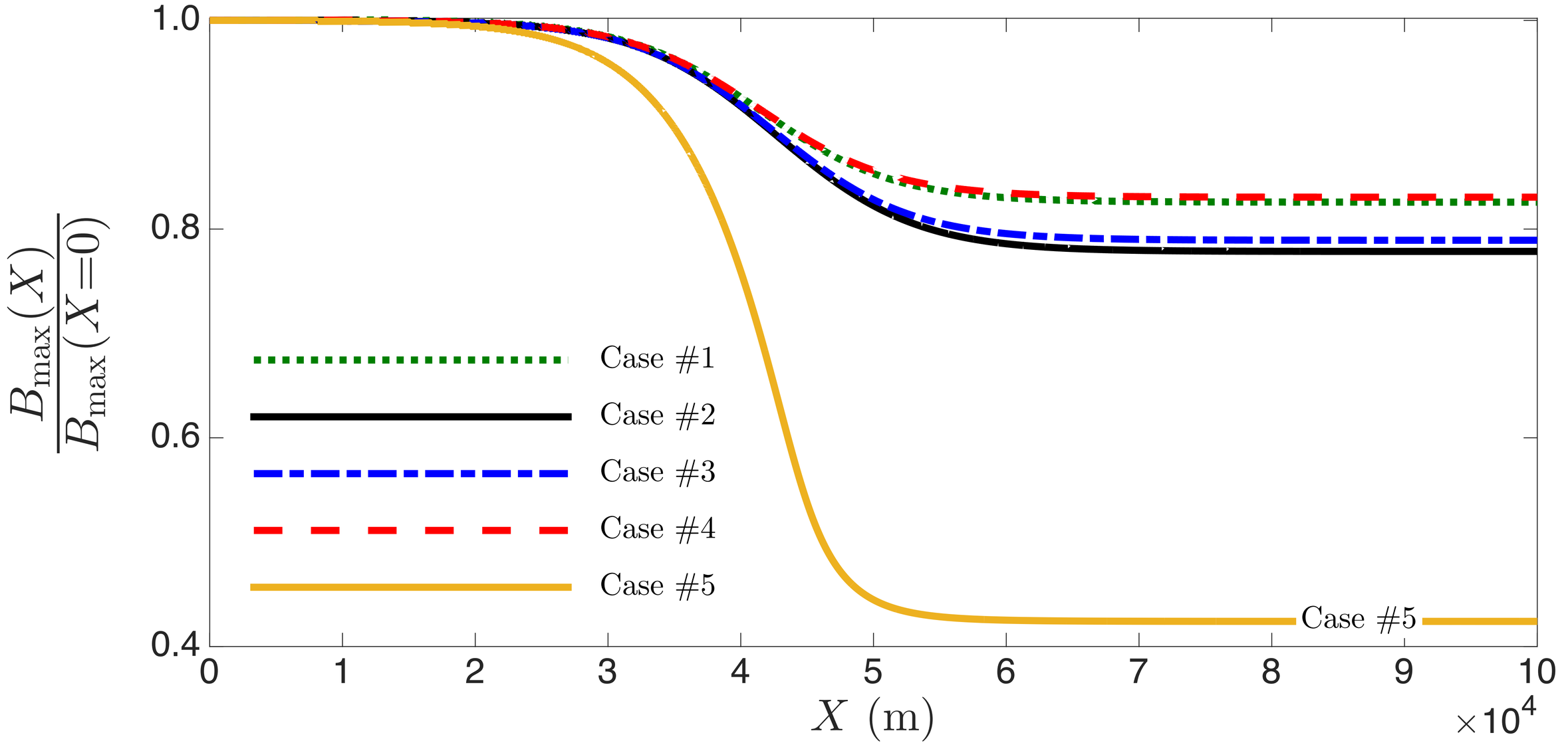

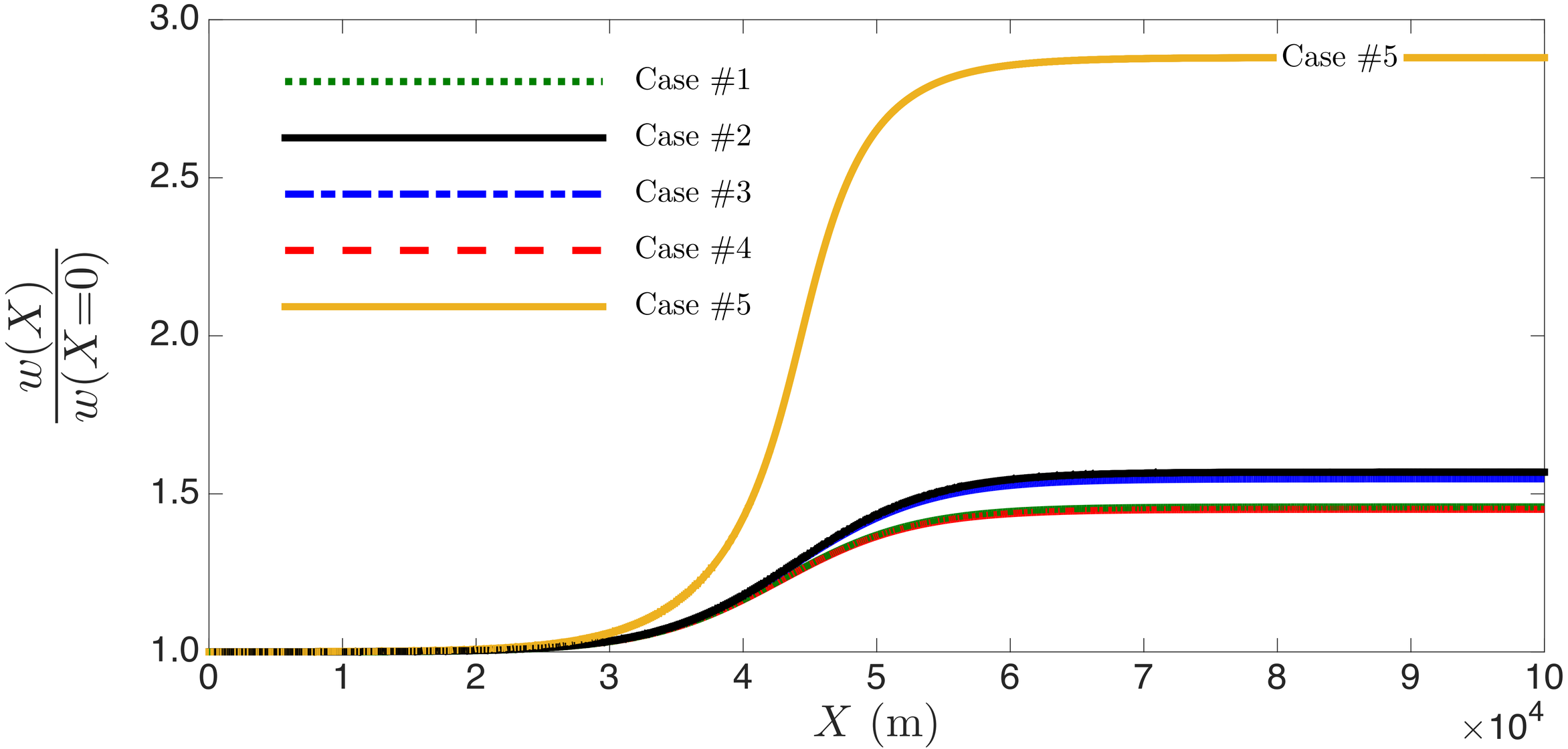

(a) (b)

(1) (2) (3) (4) (5)

$\eta(X,T)$ (m)

0.5 0 -0.5

0 2000 4000 6000

T (s)